Eur. Phys. J. C 26, 371–388 (2003)
Digital Object Identifier (DOI) 10.1140/epjc/s2002-01080-7

THE EUROPEAN PHYSICAL JOURNAL C

Coupled channel analysis of $\pi^+\pi^-\pi^0$, $K^+K^-\pi^0$ and $K^\pm K^0_S\pi^\mp$ from $\bar{p}p$ annihilation at rest in hydrogen targets at three densities

The OBELIX Collaboration

M. Bargiotti[1], A. Bertin[1], M. Bruschi[1], M. Capponi[1], S. De Castro[1], L. Fabbri[1], P. Faccioli[1], D. Galli[1], B. Giacobbe[1], U. Marconi[1], I. Massa[1], M. Piccinini[1], N. Semprini Cesari[1], R. Spighi[1], V. Vagnoni[1], S. Vecchi[1], M. Villa[1], A. Vitale[1], A. Zoccoli[1], M. Poli[2], A. Bianconi[3], M.P. Bussa[3], M. Corradini[3], A. Donzella[3], E. Lodi Rizzini[3], L. Venturelli[3], C. Cicalò[4], A. De Falco[4], A. Masoni[4], G. Puddu[4], S. Serci[4], G. Usai[4], O.E. Gorchakov[5], S.N. Prakhov[5], A.M. Rozhdestvensky[5], M.G. Sapozhnikov[5], V.I. Tretyak[5], P. Gianotti[6], C. Guaraldo[6], A. Lanaro[6], V. Lucherini[6], C. Petrascu[6], R. A. Ricci[7], V. Filippini[8], A. Fontana[8], P. Montagna[8], A. Panzarasa[9], A. Rotondi[8], P. Salvini[8], A. Zenoni[3], F. Balestra[10], L. Busso[10], P. Cerello[10], O. Denisov[10], L. Ferrero[10], R. Garfagnini[10], A. Maggiora[10], D. Panzieri[10], F. Tosello[10], E. Botta[11], T. Bressani[11], D. Calvo[11], F. De Mori[9], A. Feliciello[11], A. Filippi[11], N. Mirfakhrai[11], S. Marcello[12], M. Agnello[12], F. Iazzi[12]

[1] Dipartimento di Fisica dell'Università di Bologna and INFN Sezione di Bologna, Bologna, Italy
[2] Dipartimento di Energetica dell'Università di Firenze, Firenze, Italy and INFN Sezione di Bologna, Bologna, Italy
[3] Dipartimento di Chimica e Fisica per l'Ingegneria e per i Materiali, Università di Brescia, Brescia, Italy and INFN gruppo associato di Brescia, Brescia, Italy
[4] Dipartimento di Scienze Fisiche, Università di Cagliari and INFN Sezione di Cagliari, Cagliari, Italy
[5] Joint Institute for Nuclear Research, Dubna, Russia
[6] Lab. Naz. di Frascati dell'INFN, Frascati, Italy
[7] Lab. Naz. di Legnaro dell'INFN, Legnaro, Italy
[8] Dipartimento di Fisica Nucleare e Teorica dell'Università di Pavia and INFN Sezione di Pavia, Pavia, Italy
[9] INFN Sezione di Pavia, Pavia, Italy
[10] Dipartimento di Fisica Generale dell'Università di Torino and INFN Sezione di Torino, Torino, Italy
[11] Dipartimento di Fisica Sperimentale dell'Università di Torino and INFN Sezione di Torino, Torino, Italy
[12] Dipartimento di Fisica del Politecnico di Torino and INFN Sezione di Torino, Torino, Italy

Received: 15 July 2002 /
Published online: 9 December 2002 –

Abstract. The $\pi^+\pi^-\pi^0$, $K^+K^-\pi^0$ and $K^\pm K^0\pi^\mp$ final states produced by $\bar{p}p$ annihilation at rest at three different hydrogen target densities have been analyzed in the frame of a coupled channel analysis together with $\pi\pi$, πK and $K\bar{K}$ scattering data. The percentages of the different partial waves, the branching ratios and the parameters (masses, widths, $\pi\pi$ and $K\bar{K}$ partial widths) of all the involved resonances ($J^P = 0^+, 1^-, 2^+$) have been measured. The main results on meson spectroscopy concern the determination of the $\Gamma_{K\bar{K}}/\Gamma_{\pi\pi}$ ratio for $f_0(1370)$ and $f_0(1500)$ ($\Gamma_{K\bar{K}}/\Gamma_{\pi\pi} = 0.91 \pm 0.20$ and $\Gamma_{K\bar{K}}/\Gamma_{\pi\pi} = 0.25 \pm 0.03$ respectively), the determination of $a_0(1300)$ parameters ($M = 1303 \pm 16\,\mathrm{MeV}$; $\Gamma = 92 \pm 16\,\mathrm{MeV}$) and the observation of two different ρ signals associated to $\rho(1450)$ and $\rho(1700)$ ($M = 1182 \pm 30\,\mathrm{MeV}; \Gamma = 389 \pm 20\,\mathrm{MeV}$ and $M = 1594 \pm 20\,\mathrm{MeV}; \Gamma = 259 \pm 20\,\mathrm{MeV}$ respectively).

1 Introduction

The object of the present work is the achievement of a detailed experimental study of the following annihilation reactions at rest

$$\begin{aligned} \bar{p}p &\to \pi^+\pi^-\pi^0 \\ \bar{p}p &\to K^+K^-\pi^0 \\ \bar{p}p &\to K^\pm K^0_S\pi^\mp \end{aligned} \qquad (1)$$

measured by the OBELIX experiment at three different hydrogen target densities. Necessarily this work involves, at the same time, aspects of the atomic physics of the $\bar{p}p$ system in the hydrogen medium, of $\bar{N}N$ annihilation dynamics and of meson spectroscopy, on which the present paper is mainly focused.

From this point of view, due to the richness of the meson dynamics involved in the collected final states, different and relevant sectors of light meson spectra can be

investigated. Many prominent questions in light meson spectroscopy can be traced back to the experimental determination of $\pi\pi$ and $K\bar{K}$ decay modes, which are studied here in the frame of a coupled channel analysis. The flavour content of the exotic candidate $f_0(1500)$, the overall structure of the $J^{PC} = 0^{++}$ nonet, f_2 and ρ isobars are in fact deeply related to this issue.

The appealing features of three-meson $\bar{p}p$ annihilation at rest determine to some extent the complexity of the analysis procedure. In fact, many resonant states coupled to different hadronic channels can be produced from different isospin components and partial waves of the $\bar{p}p$ system. These considerations led us to develop an articulated approach in order to control the different features of the problem. In order to disentangle within the complicated $K^+K^-\pi^0$ dynamics the isoscalar $K\bar{K}$ contribution, also $K^\pm K^0_S\pi^\mp$ data are included. To get a better control on the difficult $J^P = 0^+$ nonet, $\pi\pi$, $K\bar{K}$ and πK scattering data were included in the analysis. A reliable identification of the different partial waves involved in $\bar{p}p$ annihilation at rest was obtained by means of an original technique developed by OBELIX: three different densities of the hydrogen target for each one of the final states studied allow for a detailed investigation of S and P-wave annihilation. Finally, the whole set of experimental data was analyzed within the frame of a coherent formalism in order to take into account the isospin and unitarity constraints which relate the different hadronic channels.

2 General approach

The $\bar{p}p$ annihilation at rest offers a natural way of limiting the number of partial waves involved in the process, which is one of the critical problems in spin-parity analyses. The mechanisms which regulate the formation and the deexcitation of the $\bar{p}p$ atom in the hydrogen medium can account for this fact [1]. After the slowing-down of one $\bar{p}$ in the hydrogen medium and the formation of a highly excited $\bar{p}p$ atom ($n \sim 30$, $l \sim 20$), the deexcitation process takes place. The competition, depending on the hydrogen density, between radiative and Stark transitions controls the final part of this process. In high density targets the compact $\bar{p}p$ atom are exposed to the electric field of the surrounding H_2 molecules. The induced Stark-mixing of the different angular momentum eigenstates rapidly leads to S-wave annihilation from high-n levels of the $\bar{p}p$ atom. On the contrary, the minor role of this mechanism in low density targets allows radiative transitions to dominate. The chain of dipolar transitions populates the 2P level from which P-wave annihilation takes place. Therefore, annihilation at rest is controlled by the incoherent superposition, given by the target density, of the $l = 0$ and $l = 1$ angular momentum eigenstates of the $\bar{p}p$ atom corresponding to six different partial waves ($^1S_0$, $^3S_1$, $^1P_1$, $^3P_0$, $^3P_1$ and $^3P_2$) in the spin-parity analysis.

The possibility of assuming a pure S-wave contribution has led many experiments to annihilate $\bar{p}$ in liquid hydrogen targets. This of course is only an approximation, which turns out to be unacceptable for high statistics data samples. In fact, the atomic cascade models [2] and the two-meson branching ratios analyses [3,4] predict in this case a P-wave contribution of the order of 10% at least. In these conditions the insertion of P-wave amplitudes, although necessary, is very difficult. In fact, the complex P-wave annihilation dynamics cannot be disentangled by means of the small contribution expected in liquid hydrogen targets. Sets of measurements with different target densities are necessary.

According to these considerations, we collected data on each final state at three different hydrogen target densities: liquid hydrogen (LH) dominated by S-wave annihilation, low density hydrogen (corresponding to a pressure of 5 mbar, LP) dominated by P-wave annihilation, and hydrogen at standard conditions of density and pressure (NP), where comparable contributions from S and P-wave annihilation are expected. As explained in Sect. 3, the inspection of the experimental data gives a direct insight of the advantages of this technique, which represents a decisive progress to get a detailed understanding of S and P-wave final state dynamics.

As it is known, for each $\bar{p}p$ partial wave, the two isospin components, with opposite G-parity, represent two different sources. No complications arise in the case of $\pi^+\pi^-\pi^0$ final state due to the fact that only $G = -1$ $\bar{p}p$ sources are involved and only $G = +1$ resonances can be produced. On the contrary both $\bar{p}p$ sources can produce the $K^+K^-\pi^0$ final state and, moreover, $G = \pm 1$ as well as undefined G-parity resonances control the final state dynamics. The case of $K^*(892)$, which is produced by ten different $\bar{p}p$ sources, is remarkable. These circumstances make the disentangling of $K^+K^-\pi^0$ dynamics a hard task and led us to consider a different charge combination of the same final state, i.e. $K^\pm K^0\pi^\mp$. As explained in Sect. 4, no additional parameters are needed to describe its dynamics; $K^*(892)$ are produced in a completely different interference pattern and, above all, the $I = 1$ $K\bar{K}$ dynamics can be studied in a situation where the $I = 0$ component is absent. This fact turns out to be crucial in extracting the $I = 0$ $K\bar{K}$ component from the $K^+K^-\pi^0$ final state. The experimental data, as explained in Sect. 3, clearly show the advantage of this approach.

Moreover, in order to obtain a coherent description of the experimental information available on the difficult $J^P = 0^+$ isobar, the $J^{PC} = 0^{++}$, $I^G = 0^+$, $\pi\pi \to \pi\pi$, $\pi\pi \to K\bar{K}$, and the $J^P = 0^+$, $I = 1/2$, $K\pi \to K\pi$ scattering data [5] were included in the present analysis.

3 Data selection

The annihilation reactions in (1) were studied on data collected by the OBELIX experiment at the Low Energy Antiproton Ring (LEAR) at CERN. The detailed description of the experimental apparatus can be found in [6]; here we recall only its main features that are necessary to understand the present paper. Inside the magnetic field provided by the Open Axial Field Magnet (0.5 T max) four subdetectors are placed:

- The Spiral Projection Chamber (SPC) acting as vertex detector. Due to the large size of the targets this detector was removed in LP and LH data taking;
- The time of flight system (TOF), consisting of two scintillator slab arrays placed around the SPC coaxially to the beam. Besides time of flight measurements, specific multiplicities and topologies of charged particles can be selected by the TOF (at trigger level);
- The Jet Drift Chamber (JDC), a cylindric detector placed inside the TOF arrays for the tracking and the identification of charged particles by means of dE/dx measurement;
- The High Angular Resolution Gamma Detector (HARGD), a system of four supermodules for the identification and the measurement of the neutral annihilation products (γs from π^0 decays).

Each annihilation channel was studied at the LH, NP and LP hydrogen target densities. To optimize the $\bar{p}$ stopping in the target center at each density, beam momenta of 200 MeV/c (LH) and 105 MeV/c (NP, LP) and materials of suitable thickness were used.

The on-line selection of the annihilation reactions in (1) was based on two main trigger setups:

- *two prong multiplicity trigger* (two hit slabs in the inner and outer part of the detector in a suitable time gate after an incoming $\bar{p}$), used to select the channels $\pi^+\pi^-\pi^0$ and $K^+K^-\pi^0$. The collected statistics amount to 10.4 (LH), 6.7 (NP) and 9.4 (LP) $\times 10^6$ events.
- *four prong multiplicity trigger*, used to select the charged particles of the channel $K^\pm K^0_S\pi^\mp$ in the $K^\pm\pi^\mp\pi^+\pi^-$ final state (through the K^0_S decay into $\pi^+\pi^-$). The data sample was enriched by means of a second level trigger request of a "slow" particle (a particle with a time-of-flight greater than 8 ns). The statistics amount to 17 (LH), 24 (NP) and 6 (LP) $\times 10^6$ events.

Once the events were reconstructed off-line by means of the general reconstruction code, the different reactions were selected by means of quality cuts and kinematic fits. As far as the selection of the $\pi^+\pi^-\pi^0$ and $K^\pm K^0_S\pi^\mp$ channels is concerned, we refer to already published results [7, 8]. Here we describe only the $K^+K^-\pi^0$ selection, which was performed through the following steps:

- two reconstructed, long tracks (in the bending plane $L_{xy} > 30cm$) of opposite charge in the JDC, originated from a vertex inside a fiducial volume contained into the target;
- an angle θ_{+-} between the charged particles momenta which satisfies the relation $cos\theta_{+-} > -0.998$. This cut rejects, almost totally, $\pi^+\pi^-$ and K^+K^- background reactions;
- charged particle identification. The identification of charged kaons, crucial in the $K^+K^-\pi^0$ final state selection, has been performed by means of the measured energy loss of the tracks in the JDC (dE/dx) and the velocity β of the particle (extrapolated to the vertex) measured by the TOF. For this reason, the analysis has been performed on selected data where these information were stable and reliable. Particular attention was dedicated to identify the kaon selection cut in the dE/dx versus $|\boldsymbol{p}|$ scatter-plot (Fig. 1a) in order to evaluate directly, on the data, the efficiency of the cut and the pion contamination. The scatter-plot was divided in slices corresponding to different momentum intervals 0.05 GeV/c wide. For each slice, the dE/dx distribution was fitted with two Landau-like functions to separate the pionic from the kaonic contribution (the proton contamination was negligible). The position of the cut in each slice was fixed to optimize a high ($\epsilon_K > 0.8$) regular efficiency on kaon selection with a low ($< 2\%$) pion contamination (Fig. 1b,c). The resulting selection cut for kaons corresponding to the NP sample is shown in Fig. 1a. The β measurement was used as an independent check on kaon identification;
- a 1C kinematic fit to test the compatibility of the selected events to the $K^+K^-\pi^0$ final state hypothesis. A selection cut on χ^2 corresponding to a confidence level of 80% was required.

The events selected contain a fraction of residual background depending on the considered channel and on the target density. In the case of the $\pi^+\pi^-\pi^0$ channel the main backgrounds, from the $\pi^+\pi^-2\pi^0$ and $\pi^+\pi^-3\pi^0$ channels (about 10%), are subtracted by means of an accurate procedure described in [9]. Concerning the $K^+K^-\pi^0$ final state, the main background contributions come from the channels $K^+K^-n\pi^0$ (rejected by kinematic fit to less than 2%), $K^\pm\pi^\mp X$, where one pion is misidentified as a kaon, and $\pi^+\pi^- X$, where both pions are confused as kaons (about $1-2\%$). Their amount and shapes on the Dalitz-plots were calculated directly on the experimental data by taking advantage of the previously explained selection based on the dE/dx. Concerning the $K^\pm K^0_S\pi^\mp$ channel, its exclusive reconstruction (all the particles in the final state are measured) and the 5C kinematic fit allows to reduce the background sources (mainly due to 5π final states) to less than 0.5% [8]. The following statistics of events survive after the described cuts and the background subtraction (in units of 10^3 events): $\pi^+\pi^-\pi^0$, 808 (LH), 420 (NP), 260 (LP); $K^+K^-\pi^0$, 20 (LH), 23 (NP), 25 (LP); $K^\pm K^0_S\pi^\mp$, 10.6 (LH), 27 (NP), 3 (LP).

The Dalitz-plots corresponding to the reactions in (1) are shown in Fig. 2. The X and Y axis are associated respectively to $\pi^+\pi^-$ and $\pi^+\pi^0$ (bin size 0.032×0.032 GeV^2), $K^+\pi^0$ and $K^-\pi^0$ (bin size 0.045×0.045 GeV^2), $K^\pm\pi^\mp$ and $K^0\pi^\mp$ (bin size 0.045×0.045 GeV^2 in LH and NP, bin size 0.090×0.090 GeV^2 in LP). In all the represented Dalitz-plots the background was subtracted but apparatus efficiency modulations have not been removed; moreover the Dalitz-plots corresponding to the first two reactions (see (1)) have been symmetrized with respect to the charge exchange. To each bin of the Dalitz-plots an error due to background subtraction and statistic fluctuations was also associated.

At first glance the dynamics of the $\pi^+\pi^-\pi^0$ channel seems to be dominated by $\rho(770)$ and $f_2(1270)$ resonances while $K^*(892)$ prevails over the $K^+K^-\pi^0$ and $K^\pm K^0_S\pi^\mp$

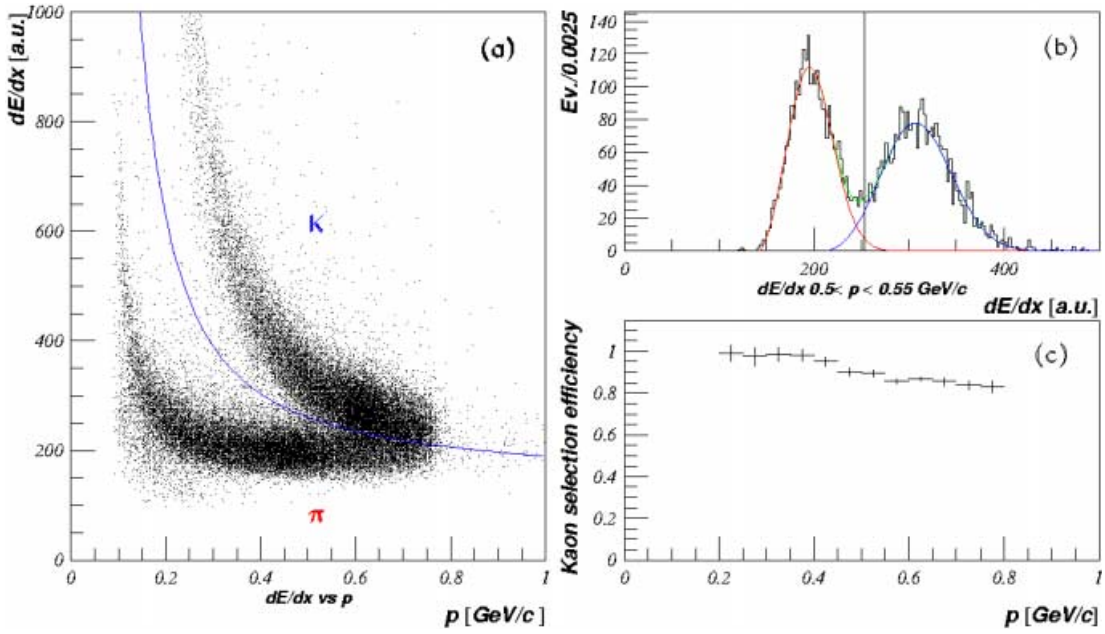

Fig. 1a–c. dE/dx versus $|\boldsymbol{p}|$ scatter plot and selection cut for kaons **a**; fit of dE/dx distributions corresponding to a fixed $|\boldsymbol{p}|$ performed by means of Landau-like distributions **b**; efficiency of the kaon selection cut **c**

final states. By looking at the figures from left to right (with decreasing hydrogen density of the target) the decrease of $\rho^0(770)$ and the enhancement of $f_2(1270)$ point out their dominant production respectively from S and P-waves of the $\bar{p}p$ system (Fig. 2 (1-a,b,c)). A dominant S-wave production is clearly shown also in the case of $\phi(1020)$ (Fig. 2 (2-a,b,c)) and $a_0(980)$ (Fig. 2 (3-a,b,c)), while P-wave controls the $f_2'(1525)$ production (Fig. 2 (2-a,b,c)). The strong concentration of events in the central region between the $K^*(892)$ bands in the $K^+K^-\pi^0$, which is absent in the $K^\pm K_S^0\pi^\mp$ final state, is due to isoscalar resonances.

An essential issue is the treatment of the apparatus efficiency and resolution, which modulate the shape and the width of the resonances. In the analyses where the bin size can be chosen to contain the resolution effects, the experimental Dalitz-plot, suitably corrected for the apparatus efficiency, can directly be compared to the theoretical amplitude. In our case the high statistics of the collected data samples suggest a bin size comparable with resolution effects so that the experimental data cannot be corrected. For this reason we decided to compare the binned experimental Dalitz-plot to the corresponding binned theoretical Dalitz-plot modulated by the apparatus efficiency and resolution

$$D^{Th'}_{p'q'} = \sum_{pq} \epsilon_{p'q',pq}\, D^{Th}_{pq} \qquad (2)$$

In this expression D^{Th}_{pq} represents the cell pq of a generic theoretical Dalitz-plot, $\epsilon_{p'q',pq}$ is the probability that an event generated in the bin pq is placed in the bin $p'q'$ and $D^{Th'}_{jk}$ is the transformed theoretical Dalitz-plot. The numerical values of $\epsilon_{p'q',pq}$ were obtained by means of a detailed Monte Carlo simulation of the whole experimental setup (beam distribution, target density, detector configurations, responses and efficiencies, trigger setup and performances, etc.) for each analyzed data sample. In order to have an accurate representation of the efficiency and resolution effects the simulated events were submitted to the same selection chain used for experimental data.

4 The description of $\bar{p}p$ annihilation at rest

The sequence of processes which take place in $\bar{p}p$ annihilation at rest in liquid or gaseous hydrogen are sketched in Fig. 3.

After the slowing down in hydrogen, the $\bar{p}$ undergoes atomic capture giving place to a highly excitated protonium atom. The mechanisms discussed in Sect. 2 determines the percentages of atoms with angular momenta $l = 0, 1$ and hence the percentages $W^k(\rho_t)$ of the hyperfine levels involved in $\bar{p}p$ annihilation at rest: $^1S_0$, $^3S_1$, $^1P_1$, $^3P_0$ (forbidden for annihilation in three pseudoscalar mesons), $^3P_1$ and $^3P_2$. All the atomic physics involved in our problem is described by these parameters. The decrease of centrifugal barriers effects in $l = 0, 1$ angular momentum states leads the system to annihilation. It is usually believed that this process can de-couple the initial from the final state. In this way the observed dynamics is entirely due to the reciprocal interactions of the produced mesons (*Final State Interaction* hypothesis) [10]. The structure of these hadronic processes (discussed in detail in the following) are represented by means of a series of poles. Each pole is coupled to the $\bar{p}p$ system by the so called production parameters β^k_α and can decay into stable mesonic couples j via the decay constant $g_{\alpha j}$ (for convenience in the following j will also be used to indicate the whole final state). According to the *Isobar Model* hypothesis [11], the third stable meson does not take part

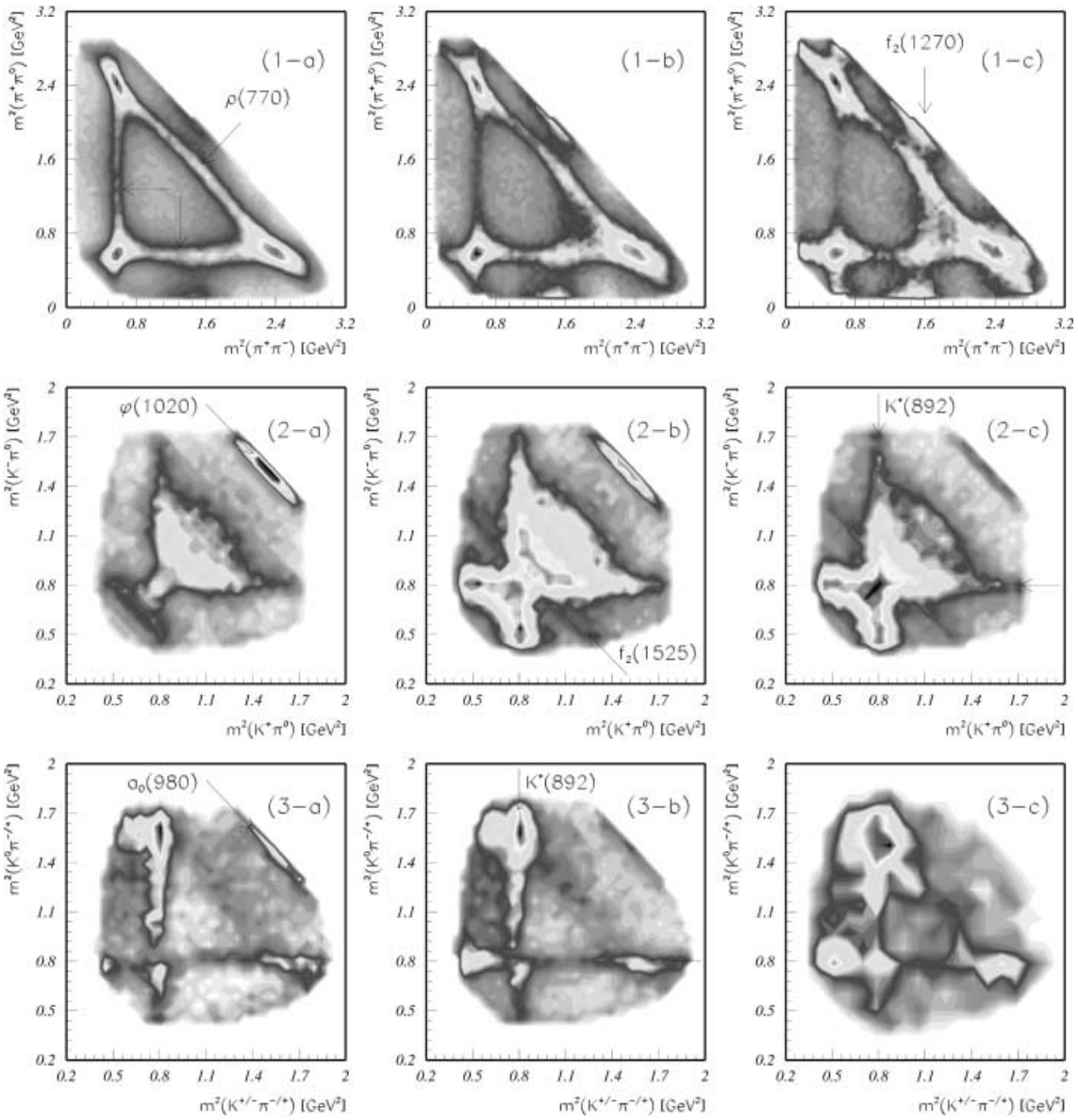

Fig. 2. Dalitz-plots (background subtracted) of the annihilation reactions $\bar{p}p \to \pi^+\pi^-\pi^0$ (first row), $\bar{p}p \to K^+K^-\pi^0$ (second row) and $\bar{p}p \to K^\pm K^0_S\pi^\mp$ (third row) in liquid **a**, NP gas **b** and low pressure gas **c** hydrogen targets. The details are discussed in the text.

in the final state process dynamics, limiting its contribution to the initial state dynamics. The expected number of events in the bin pq of the Dalitz-plot corresponding to the final state j can be written as

$$D^{Th}_{pq\,j}(\rho_t) \;=\; \sum_{k=1}^{N_{pw}} f^k_j(\rho_t)|\mathcal{F}^k_{pq\,j}|^2 \qquad (3)$$

where N_{pw} is the number of partial waves and $\mathcal{F}^k_{pq\,j}$ are the partial wave amplitudes. The coefficients $f^k_j(\rho_t)$ depend on the number $N_j(\rho_t)$ of events in each channel, on the hyperfine level percentages $W^k(\rho_t)$ and, since we normalize the production parameters to a given resonance in each partial wave, on the absolute normalization $\hat{\beta}^k$ of the production parameters:

$$f^k_j(\rho_t) \;=\; N_j(\rho_t)\, W^k(\rho_t)\, |\hat{\beta}^k|^2 \qquad (4)$$

These parameters are fitted to the experimental data together with the production parameters β^k_α, the pole masses m_α and the decay constants $g_{\alpha j}$. Several constraints limit the number of independent $f^k_j(\rho_t)$. By comparing the $f^k_j(\rho_t)$ corresponding to different final states we get the ratio

$$\frac{f^k_j(\rho_t)}{f^k_l(\rho_t)} \;=\; \frac{N_j(\rho_t)}{N_l(\rho_t)} \;=\; C_{jl}(\rho_t) \qquad (5)$$

which reduces the number of independent $f^k_j(\rho_t)$ (in our case 3 final states at 3 densities, each with 5 partial waves, correspond to 45 parameters. They reduce to 3×5+3+3 independent values if constraints are applied).

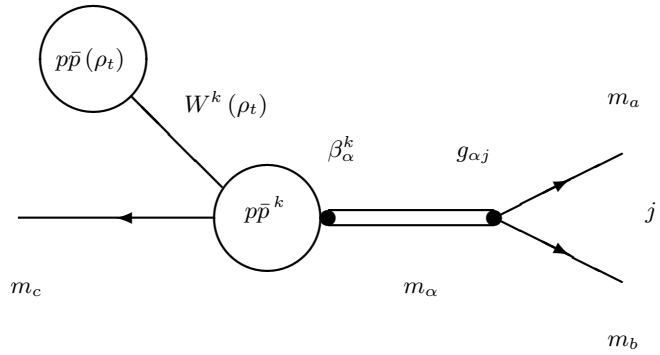

Fig. 3. Schematic representation of the processes involved in $\bar{p}p$ annihilation at rest

The partial wave amplitude (labelled in this formula by means of all quantum numbers) into the final state j is written as the sum of two-body reaction terms extended to all the possible couples of final mesons

$$\begin{aligned}\mathcal{F}_j^{^{2S+1}L_J,II_3} \;=\; \sum_{ab}\; & C\;{}^{II_3}_{I^{ab}I_3^{ab},I^cI_3^c} \\ & Z\;{}^{JJ_3}_{L^{ab}L_3^{ab},L^cL_3^c}(\hat{\boldsymbol{p}},\hat{\boldsymbol{q}}')\,B_{L^c}(|\boldsymbol{p}|) \\ & F\;{}^{L^{ab},I^{ab}I_3^{ab}}_{j}(|\boldsymbol{q}'|) \end{aligned} \qquad (6)$$

where I^{ab}, L^{ab}, I^c and L^c are the isospin and the angular momentum of the isobar and the spectator respectively; I, I_3, J and J_3 the isospin and the angular momentum (with the respective third components) of $\bar{p}p$ system. The sum runs over all the quantum numbers allowed by the selection rules of the process i.e. angular momentum, parity, isospin, G-parity and strangeness (see Tables 5–9 in appendix). The involved particles are grouped in isospin multiplets and $C^{II_3}_{I^{ab}I_3^{ab},I^cI_3^c}$ represent the Clebsh-Gordan coefficients associated to the isospin projection of the initial state on the intermediate state and have to be calculated consistently in order to represent correctly the interference effects especially in the kaonic final states (see Tables 5–9). Angular momentum states are described by normalized Zemach tensors [13] constructed by means of the spectator momentum versor $\hat{\boldsymbol{p}}$ in the laboratory frame (to represent resonance-spectator relative angular momentum) and the decay momentum versor $\hat{q'}$ in the resonance frame (to represent the resonance spin). Projections are calculated according to the rules of tensorial calculus. The use of normalized Zemach tensors is justified by the necessity of having an accurate centrifugal barrier description. Here we assume the Blatt-Weisskopf centrifugal barriers [14].

$F_j^{L^{ab},I^{ab}I_3^{ab}}(|\boldsymbol{q}'|)$ represents the relativistic production amplitude of the annihilation process, its expression in the frame of the K-matrix and P-vector [20] approach is given by the equation (the upper indices $L^{ab}, I^{ab}I_3^{ab}$ will be substituted by k in the following)

$$F^k \;=\; P^k\,(1 - i\,\rho\,K)^{-1} \qquad T \;=\; K\,(1 - i\,\rho\,K)^{-1} \qquad (7)$$

where the diagonal matrix ρ describes the densities of final state. If pairs of stable mesons are produced in the channel j, the following formula is used

$$\rho_{jj}(m) = \sqrt{(1 - \frac{(m_{ja}+m_{jb})^2}{m^2})(1 - \frac{(m_{ja}-m_{jb})^2}{m^2})} \qquad (8)$$

where m_{ja} and m_{jb} are meson masses and $m = \sqrt{s}$ is the invariant mass. In the case of the 4π decay mode, dominated by $\rho\rho$, $\sigma\sigma$ or $\rho\sigma$ intermediate states, we use the expression of [15]. Below each physical threshold, we use the analytic continuation of ρ_{jj} in order to take into account the analytic properties of the amplitude.

The elements of the P^k vectors and of the K matrix are given by the expressions

$$P_j^k = \sum_{\alpha=1}^{N_p} \frac{\beta_\alpha^k\, g_{\alpha j}\, B_{\alpha j}}{m_\alpha^2 \,-\, m^2} + d_j^k \qquad (9)$$

$$K_{jl} = \left(\sum_{\alpha=1}^{N_p} \frac{g_{\alpha j}\, g_{\alpha l}\, B_{\alpha j}\, B_{\alpha l}}{m_\alpha^2 \,-\, m^2} + c_{jl}\right) Z$$

where the invariant mass function $Z = (2m^2 - m_\pi^2)/2m^2$ is introduced in the $\pi\pi$ and $K\pi$ S-wave scattering amplitudes [15] to account for Adler zero [16], elsewhere it is set to one. $B_{\alpha j} = B_{L^{ab}}(|\boldsymbol{q}'|)/B_{L^{ab}}(|\boldsymbol{q}'_\alpha|)$ are the Blatt-Weisskopf centrifugal barriers normalized to the unit on the resonance breakup momentum $\boldsymbol{q}'_\alpha$ [14].

According to the final state interaction and isobar model, the production parameters β_α^k are real constants [17], nevertheless, to include possible violations of this scheme, complex values are allowed [18]. The couplings $g_{\alpha j}$ of the pole α to the final state j (assumed real in order to satisfy the unitarity of T operator) are expressed by real numbers in the case of $J^{PC} = 0^{++}, I^G = 0^+$ isobar while the following formula is adopted in all other cases:

$$g_{\alpha j} \;=\; \sqrt{\frac{m_\alpha\,\gamma_{\alpha j}}{\rho_{jj}(m_\alpha)}} \qquad (10)$$

where $\rho_{jj}(m_\alpha)$ is the final state density calculated at the pole mass value m_α (see (8)). The background parameters used for the $J^{PC} = 0^{++}, I^G = 0^+$ isobar, have the following expressions [15]:

$$d_j^k \;=\; \phi_j^k\,\frac{1+s_0}{s_0+m^2} \qquad c_{jl} \;=\; f_{jl}\,\frac{1+s_0}{s_0+m^2} \qquad (11)$$

where ϕ_j^k, s_0 and f_{jl} are free parameters. In the case of $J^P = 0^+, I^G = 1/2$ isobar we used expression given by the scattering length approximation.

As said previously, the K-matrix and P-vector approach allows a unified description of production and scattering processes so that, independently on the process used to produce the resonances, all the data can be analyzed together. In the present analysis, scattering data are included in the case of $J^{PC} = 0^{++}, I^G = 0^+$ ($\pi\pi$ and $K\bar{K}$ scattering) and $J^P = 0^+, I = 1/2$ isobars ($K\pi$ scattering) [5] (see Fig. 5). Phases and inelasticities can be obtained by the matrix elements of the non-relativistic transition operator $T^{NR} = \rho\,T\,\rho$ (7) by means of the following equation

$$S_{ij} \;=\; \delta_{ij} + 2\,i\,T_{ij}^{NR} \;=\; \eta_{ij}\,e^{2\,i\,\theta_{ij}} \qquad (12)$$

5 Fit results

The fit of the theoretical functions (2) and (12) to the experimental data is performed by means of the least-square method. The expression for the χ^2 function is the following:

$$\chi^2 = \sum_\alpha \lambda_\alpha \sum_{pq} \frac{(D^{Th'}_{pq\,\alpha} - D^{Exp}_{pq\,\alpha})^2}{(\epsilon D^{Th'}_{pq\,\alpha})^2 + (\epsilon D^{Exp}_{pq\,\alpha})^2} + \sum_\alpha \lambda_\alpha \sum_{p} \frac{(\delta^{Th}_{p\,\alpha} - \delta^{Exp}_{p\,\alpha})^2}{(\epsilon\delta^{Exp}_{p\,\alpha})^2} \quad (13)$$

In this formula α runs over all nine experimental Dalitz-plots in the first sum and over the set of scattering data included in the present analysis in the second sum; pq run over the experimental Dalitz-plot cells in the first sum and p runs over the experimental scattering points in the second sum; $D^{Th'}_{pq\,\alpha}$ and $\epsilon D^{Th'}_{pq\,\alpha}$, $D^{Exp}_{pq\,\alpha}$ and $\epsilon D^{Exp}_{pq\,\alpha}$, $\delta^{Th}_{p\,\alpha}$ and $\epsilon\delta^{Th}_{p\,\alpha}$, $\delta^{Exp}_{p\,\alpha}$ and $\epsilon\delta^{Exp}_{p\,\alpha}$ represent the values of the theoretical functions and the content of the experimental bins with the errors for annihilation and scattering data respectively; the factors λ_α are used to equalize the contribution of each fitted data sample to the χ^2 function.

To define the theoretical amplitude the isobars, the number of poles in each isobar and their decay channels need to be defined. As said in Sect. 2, the experimental conditions limit the orbital angular momentum values of the $\bar{p}p$ system to $l = 0, 1$ so that the following initial states are allowed: $^1S_0$, $^3S_1$, $^1P_1$, $^3P_1$, $^3P_2$, each one with isospin $I = 0, 1$ (in three pseudoscalar meson final states $^3P_0$ is ruled out by P conservation). Concerning the resonance quantum numbers, we include only the $I = 0, 1/2, 1$ isospins. The weak $I = 2$ signal observed by Obelix in the annihilation reaction $\bar{n}p \to \pi^+\pi^+\pi^-$ in $\pi^+\pi^+$ invariant mass [31] is not considered since, in our case, $\pi^+\pi^-$ and $\pi^\pm\pi^0$ invariant masses are dominated by $I = 0, 1$ contributions. Concerning the spin we are guided by the consideration that below 1700 MeV mass (limit fixed by energy-momentum conservation) meson dynamics is almost completely dominated by $J^P = 0^+$, 1^-, and 2^+ quantum numbers so that higher value spins are not considered. Since centrifugal barrier effects suppress high angular momenta, the limit $L \leq 2$ is assumed on the resonance-spectator relative orbital angular momentum. These considerations, together with the systematic application of the selection rules, lead to the detailed tables shown in appendix where the spin, the relative angular momentum and the interference patterns of the possible resonances are listed for each $\bar{p}p$ initial state.

As far as the poles included in the involved isobars are concerned the detailed structure is discussed in the following and reported in Table 1.

- f_0 *isobar.* The contribution of $f_0(980)$ pole plus a non-resonant background is clearly required by the direct inspection of the $\theta_0(\pi\pi \to \pi\pi)$ phase shift. Annihilation data require clearly at least two additional poles. In this configuration, adopted also in our previous analysis of the $\pi^+\pi^-\pi^0$ final state [7], we get a broad $f_0(1370)$ and a relatively narrow $f_0(1500)$. In the present analysis, as suggested by [15], we introduced a fourth pole which improves the data description and produces the splitting of the broad $f_0(1370)$ into a broad $f_0(400-1200)$ and a relatively narrow $f_0(1370)$. A five pole amplitude, including also the $f_0(1710)$, seems not to be required by the data. Due to the absence of relative angular momentum between the decaying mesons, the threshold effects in this isobar are particularly strong. For this reason $\pi\pi$, $K\bar{K}$, $\eta\eta$ and 4π thresholds have been included separately.
- K^*_0 *isobar.* Besides the annihilation data samples, the pole structure is defined by $K\pi$ scattering data which require the contribution of the non-resonant background and of the $K^*_0(1430)$ pole. Only the $K\pi$ decay channel was considered.
- a_0 *isobar.* The low $K^\pm K^0_S$ invariant mass region is the most evident proof of the existence of $a_0(980)$. $K\bar{K}$ and $\eta\pi$ decay modes were introduced to account for its production nearby $K\bar{K}$ threshold. A second pole $a_0(1300)$ is required especially by $K^\pm K^0_S\pi^\mp$ data in the steep slope of $a_2(1320)$ signal. Different mass values has been considered but they do not produce any significative χ^2 improvement. Only the $K\bar{K}$ decay channel, directly measurable in the present analysis, was considered.
- ϕ *isobar.* Besides the $\phi(1020)$ pole visible in the low energy region of K^+K^- invariant mass we tested also the $\phi(1680)$ pole: this turns out to be not necessary to fit the data and hence has been removed. Only the $K\bar{K}$ decay channel was included.
- K^*_1 *isobar.* Besides the $K^*_1(892)$ pole which dominates $K\bar{K}\pi$ dynamics we tested also the $K^*_1(1410)$ pole which is not necessary to fit the data and hence has been removed. Only the $K\pi$ decay channel was included.
- ρ *isobar.* Apart from the huge $\rho(770)$ signal, we include the $\rho(1450)$ pole required by $\pi^+\pi^-\pi^0$ data samples especially in the low $\pi^+\pi^-$ invariant mass region of the Dalitz-plots (this signal is responsible for the bending of the $\rho(770)$ shape). A third $\rho(1700)$ pole is strongly required by $K\bar{K}\pi$ data samples to avoid strong systematic deviations in the high K^+K^- and $K^\pm K^0$ invariant mass region (spin 0 and 2 were rejected by χ^2 test). The couplings included were $\pi\pi$, $K\bar{K}$ and 4π.
- f_2 *isobar.* The $f_2(1270)$ and $f'_2(1525)$ poles are clearly visible in the Dalitz-plots of $\pi^+\pi^-\pi^0$ and $K^+K^-\pi^0$ final states. An additional $f_2(1565)$ pole is required by NP and LP $\pi^+\pi^-\pi^0$ data samples mainly from $^3P_2$ partial wave annihilation. In order to introduce in the analysis of this controversial signal only measurable parameters we decide to open only $\pi\pi$ and $K\bar{K}$ decay modes.
- K^*_2 *isobar.* The $K^*_2(1430)$ pole was not included because it is out of the available $K\pi$ kinematic region.
- a_2 *isobar.* Only the $a_2(1320)$ pole is necessary. Only the $K\bar{K}$ channel is included since the dominant $\rho\pi$ and $\eta\pi$ decays do not introduce visible thresholds effects to the $K\bar{K}$ mode, neither reduce the importance or change the parameters of $a_0(1300)$.

Table 1. K-matrix and T-matrix parameters of the poles corresponding to the best fit solution. All values except f are expressed in MeV units. Errors accounts for statistical and systematical deviations. Values without errors are assumed fixed. (*) Decay channels whose experimental data are not included in the analysis. (^{a}) Values not corrected for the real $K\bar{K}$ phase space

Resonance	*K-matrix Parameters*			*T-matrix Parameters*			
	Mass	*Coupling*		*M*	*Γ*	*Partial Width*	
$f_0(980)$	422 ± 35	$g_{\pi\pi}$	1298 ± 20	984 ± 15	29 ± 14	$\Gamma_{\pi\pi}$	21 ± 7
		$g_{K\bar{K}}$	-1101 ± 25			$\Gamma_{K\bar{K}}$	5.4 ± 2
		$g_{\eta\eta}$	-162 ± 80			$\Gamma_{\eta\eta}$	$2.2 \pm 1^*$
		$g_{4\pi}$	0			$\Gamma_{4\pi}$	$0.1 \pm 0.04^*$
$f_0(400{-}1200)$	1217 ± 25	$g_{\pi\pi}$	931 ± 10	1597 ± 30	726 ± 40	$\Gamma_{\pi\pi}$	602 ± 30
		$g_{K\bar{K}}$	584 ± 20			$\Gamma_{K\bar{K}}$	120 ± 20
		$g_{\eta\eta}$	95 ± 60			$\Gamma_{\eta\eta}$	$0.4 \pm 0.2^*$
		$g_{4\pi}$	0			$\Gamma_{4\pi}$	$3.5 \pm 1.0^*$
$f_0(1370)$	1353 ± 17	$g_{\pi\pi}$	65 ± 6	1373 ± 15	274 ± 20	$\Gamma_{\pi\pi}$	10.8 ± 2
		$g_{K\bar{K}}$	41 ± 6			$\Gamma_{K\bar{K}}$	9.8 ± 2
		$g_{\eta\eta}$	504 ± 150			$\Gamma_{\eta\eta}$	$107 \pm 10^*$
		$g_{4\pi}$	406 ± 25			$\Gamma_{4\pi}$	$146 \pm 12^*$
$f_0(1500)$	1573 ± 10	$g_{\pi\pi}$	487 ± 30	1484 ± 10	125 ± 12	$\Gamma_{\pi\pi}$	35.8 ± 4
		$g_{K\bar{K}}$	44 ± 8			$\Gamma_{K\bar{K}}$	9.0 ± 2
		$g_{\eta\eta}$	278 ± 40			$\Gamma_{\eta\eta}$	$26.6 \pm 4^*$
		$g_{4\pi}$	367 ± 30			$\Gamma_{4\pi}$	$54 \pm 8^*$
		f_{11}	0.61 ± 0.07				
		f_{12}	-0.86 ± 0.04				
		s_0	1.68 ± 0.07				
$K_0^*(1430)$	1327 ± 10	$\gamma_{\pi K}$	429 ± 5	1436 ± 30	288 ± 35	$\Gamma_{\pi K}$	288 ± 35
		f	1.48 ± 0.34				
		s_0	3.7 ± 0.7				
$a_0(980)$	1000 ± 6	$\gamma_{K\bar{K}}$	26 ± 3	998 ± 10	72 ± 15	$\Gamma_{K\bar{K}}$	26 ± 6^a
		$\gamma_{\pi\eta}$	44 ± 6			$\Gamma_{\pi\eta}$	$46 \pm 8^*$
$a_0(1300)$	1311 ± 14	$\gamma_{K\bar{K}}$	94 ± 12	1303 ± 16	92 ± 16	$\Gamma_{K\bar{K}}$	91 ± 15
		$\gamma_{\pi\eta}$	0			$\Gamma_{\pi\eta}$	$1 \pm 0.5^*$
$\phi(1020)$	1019 ± 6	$\gamma_{K\bar{K}}$	3.7 ± 0.5	1019 ± 6	3.7 ± 0.5	$\Gamma_{K\bar{K}}$	3.7 ± 0.5
$K_1^{*\pm}(892)$	895 ± 4	$\gamma_{\pi K}$	53 ± 1	895 ± 2	53 ± 4	$\Gamma_{\pi K}$	53 ± 1
$K_1^{*0}(892)$	899 ± 4	$\gamma_{\pi K}$	55 ± 2	899 ± 3	55 ± 4	$\Gamma_{\pi K}$	55 ± 2
$\rho^{\pm}(770)$	743 ± 5	$\gamma_{\pi\pi}$	131 ± 9	754 ± 5	132 ± 10	$\Gamma_{\pi\pi}$	132 ± 10
		$\gamma_{K\bar{K}}$	0			$\Gamma_{K\bar{K}}$	0
		$\gamma_{4\pi}$	0			$\Gamma_{4\pi}$	$< 0.02^*$
$\rho^0(770)$	738 ± 5	$\gamma_{\pi\pi}$	144 ± 7	752 ± 5	145 ± 10	$\Gamma_{\pi\pi}$	145 ± 10
		$\gamma_{K\bar{K}}$	0			$\Gamma_{K\bar{K}}$	0
		$\gamma_{4\pi}$	0			$\Gamma_{4\pi}$	$< 0.02^*$
$\rho(1450)$	1158 ± 35	$\gamma_{\pi\pi}$	172 ± 20	1182 ± 30	389 ± 20	$\Gamma_{\pi\pi}$	187 ± 14
		$\gamma_{K\bar{K}}$	< 0.01			$\Gamma_{K\bar{K}}$	< 3
		$\gamma_{4\pi}$	202 ± 20			$\Gamma_{4\pi}$	$209 \pm 14^*$
$\rho(1700)$	1624 ± 15	$\gamma_{\pi\pi}$	10 ± 2	1594 ± 20	259 ± 20	$\Gamma_{\pi\pi}$	18 ± 5
		$\gamma_{K\bar{K}}$	60 ± 5			$\Gamma_{K\bar{K}}$	55 ± 12
		$\gamma_{4\pi}$	191 ± 10			$\Gamma_{4\pi}$	$236 \pm 14^*$
$f_2(1270)$	1221 ± 9	$\gamma_{\pi\pi}$	159 ± 10	1251 ± 7	192 ± 10	$\Gamma_{\pi\pi}$	165 ± 9
		$\gamma_{K\bar{K}}$	6.6 ± 1.0			$\Gamma_{K\bar{K}}$	7.5 ± 2
		$\gamma_{4\pi}$	20 ± 5			$\Gamma_{4\pi}$	$19 \pm 9^*$
$f_2'(1525)$	1522 ± 8	$\gamma_{\pi\pi}$	0	1521 ± 7	68 ± 7	$\Gamma_{\pi\pi}$	< 0.1
		$\gamma_{K\bar{K}}$	68 ± 8			$\Gamma_{K\bar{K}}$	68 ± 8
		$\gamma_{4\pi}$	0			$\Gamma_{4\pi}$	$< 0.1^*$
$f_2(1565)$	1520 ± 20	$\gamma_{\pi\pi}$	205 ± 20	1489 ± 15	204 ± 20	$\Gamma_{\pi\pi}$	$-$
		$\gamma_{K\bar{K}}$	0			$\Gamma_{K\bar{K}}$	$-$
		$\gamma_{4\pi}$	0			$\Gamma_{4\pi}$	$-$
$a_2(1320)$	1319 ± 10	$\gamma_{K\bar{K}}$	136 ± 25	1319 ± 10	136 ± 25	$\Gamma_{K\bar{K}}$	$-$

Table 2. Branching ratios $BR_j(\rho_t)$ and partial wave percentages $\mathcal{P}_j^k(\rho_t)$ of the analyzed $\bar{p}p$ annihilation reactions. The values correspond to the best fit solution, the errors account for statistic and systematic deviations

Reaction	ρ_t	$BR \times 10^{-3}$	$^1S_0$	$^3S_1$	$^1P_1$	$^3P_1$	$^3P_2$
$p\bar{p} \to \pi^+\pi^-\pi^0$	LH	$53.6 \pm 2.7^{[32]}$	17.6 ± 1.0	66.7 ± 1.5	$< 0.1^{+0.7}_{-0.1}$	10.2 ± 1.1	5.4 ± 0.5
	NP	$51.6 \pm 2.6^{[32]}$	9.5 ± 0.7	35.9 ± 1.0	19.2 ± 1.3	23.2 ± 1.5	12.2 ± 1.2
	LP	$48.9 \pm 2.8^{[32]}$	4.3 ± 1.0	16.2 ± 1.3	27.9 ± 2.0	33.8 ± 1.9	17.8 ± 2.0
$p\bar{p} \to K^+K^-\pi^0$	LH	$2.37 \pm 0.16^{[32]}$	38.0 ± 1.8	37.7 ± 1.9	$< 0.1^{+0.9}_{-0.1}$	17.3 ± 1.7	6.9 ± 2.1
	NP	$3.03 \pm 0.20^{[32]}$	17.3 ± 1.4	17.1 ± 0.8	18.9 ± 2.5	33.4 ± 1.8	13.3 ± 4.0
	LP	$3.15 \pm 0.22^{[32]}$	7.0 ± 1.1	7.0 ± 0.4	24.8 ± 3.5	43.8 ± 3.0	17.4 ± 5.0
$p\bar{p} \to K^\pm K^0_S \pi^\mp$	LH	$3.16 \pm 0.40^{[8]}$	35.3 ± 1.7	34.4 ± 1.9	$0.2^{+1.7}_{-0.2}$	19.1 ± 2.2	11.0 ± 2.0
	NP	$3.64 \pm 0.50^{[8]}$	12.3 ± 1.0	11.9 ± 0.7	31.8 ± 3.2	27.9 ± 2.5	16.1 ± 2.8
	LP	$4.32 \pm 0.60^{[8]}$	4.6 ± 0.7	4.4 ± 0.3	38.1 ± 3.5	33.5 ± 2.9	19.4 ± 3.5

The best fit solution we present was obtained after a long series of different fits with different hypotheses, constraints and initial values. The solution found matches both the best χ^2 criterion and some consistency checks we will discuss in the following section. In Fig. 4 the neutral and charged $\pi\pi$, $K\bar{K}$ and $K\pi$ invariant mass projections of the Dalitz-plots corresponding to the best fit solution are represented; the errors on the binned theoretical functions (shaded histograms) are summed to the experimental ones.

The reduced $\chi^2/n.d.f.$ turns out to be: 1.34 (LH), 1.27 (NP) and 1.49 (LP) for the $\pi^+\pi^-\pi^0$; 1.22 (LH), 1.06 (NP) and 1.17 (LP) for the $K^+K^-\pi^0$ and 0.94 (LH), 1.07 (NP) and 0.76 (LP) for the $K^\pm K^0_S\pi^\mp$ final states without any systematic deviations of χ^2 visible on the Dalitz-plots. Possible deviations in the invariant mass projections are due to the squared composition of the errors of the Dalitz-plot bins. In Fig. 5 are plotted phase shifts and inelasticities of the scattering data. The following reduced $\chi^2/n.d.f.$ for phases and inelasticities are obtained: 0.92, 1.08 for $\pi\pi \to \pi\pi$; 0.78, 1.58 for $K\pi \to K\pi$ and 1.13, 0.8 for $\pi\pi \to K\bar{K}$ respectively.

The values of K-matrix masses and couplings, listed in the second and third column of Table 1, correspond to the best fit solution. In the fourth and fifth column the physical state masses and widths are listed. The quoted errors account for statistic and systematic deviations and are evaluated on a selected set of fits. The values quoted without errors are assumed to be fixed. The resonance values are usually obtained by looking for T-operator singularities in the complex energy plane [19]. Here we used a different method based on the diagonalization of T and F operators discussed in [12] by which it is possible to obtain, besides the masses and total widths of the physical states, also their partial widths.

6 Discussion of the results

6.1 Partial wave percentages

The $\bar{p}p$ partial wave percentages are obtained from (3) and (4) by means of the formula

$$\begin{aligned}\mathcal{P}_j^k(\rho_t) &= \frac{W^k(\rho_t)\,|\hat{\beta}^k|^2 \sum_{pq} |\mathcal{F}^k_{pq\,j}|^2}{\sum_{l=1}^{N_{pw}} W^l(\rho_t)\,|\hat{\beta}^l|^2 \sum_{pq} |\mathcal{F}^l_{pq\,j}|^2} \\ &= \frac{W^k(\rho_t)\,BR_j^k}{\sum_{l=1}^{N_{pw}} W^l(\rho_t)\,BR_j^l} \end{aligned} \quad (14)$$

where the pq sums are performed over the Dalitz-plot cells of the final state j and partial wave k and BR_j^k represent the corresponding hadronic branching ratios. It is easy to verify that the denominator represents the branching ratio $BR_j(\rho_t)$ of the final state j at the density ρ_t which can be determined experimentally.

The annihilation branching ratios of the analyzed final states previously measured by Obelix [8,32] and the corresponding partial wave percentages obtained by the present analysis are listed in Table 2. As expected, a strong modulation of S and P-wave contributions due to the variation of hydrogen density is observed. Despite this, it is clear that the P-wave contribution cannot be neglected in liquid hydrogen targets as well as the S-wave in low density ones. This fact shows the intrinsic limit of the analyses performed with LH data only: the P-wave contribution turns out to be too weak to be correctly determined although too strong to be neglected.

The multiplication of $BR_j(\rho_t)$ and $\mathcal{P}_j^k(\rho_t)$ gives the products $W_k(\rho_t)\,BR_j^k$ from which we extract the density dependence of the $\bar{p}p$ annihilation frequency $W_k(\rho_t)$ from each final state independently. In the case of $^1S_0$ and $^3S_1$ partial waves this dependence can be extracted also from $\bar{p}p \to K^\pm K^0 \pi^\mp \pi^+ \pi^-$ spin-parity analysis [22] and from the branching ratio of $\bar{p}p \to K_S K_L$ [21], both performed at different hydrogen densities. The consistency among the determinations obtained from the different final states and the agreement with the independent experimental determination of the $\eta(1440)\pi^+\pi^-$ and K_SK_L branching ratios proves the reliability of the obtained partial wave deconvolution (Fig. 6). The density dependence of $W_k(\rho_t)$ can be extracted also from [3]. The two curves represented in Fig. 6 interpolate five points given in the paper and limit the region allowed by the different models considered. Reminding that our $W_k(\rho_t)$ are determined with an arbitrary

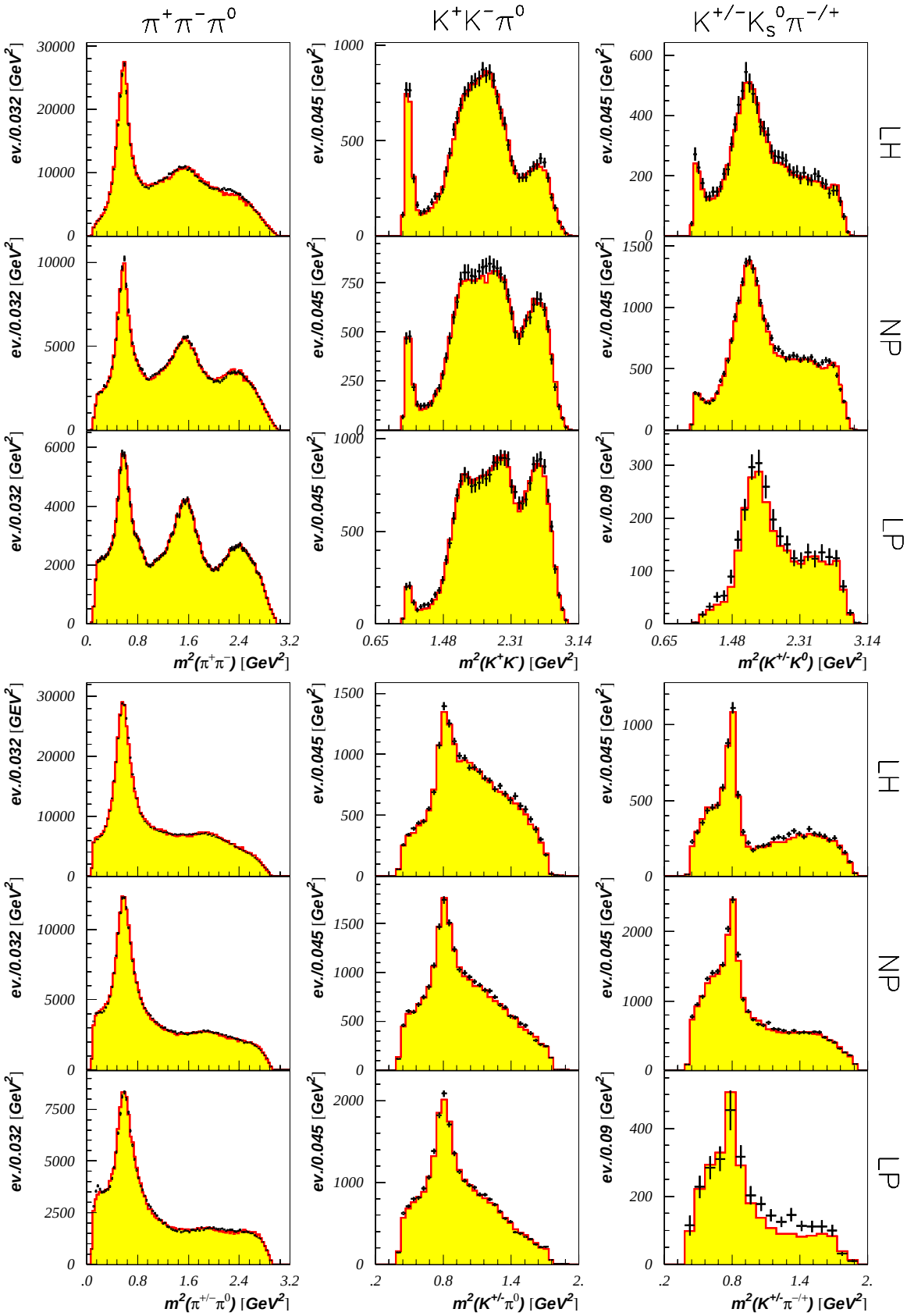

Fig. 4. Theoretical (shaded histograms) and experimental (background subtracted) Dalitz-plot projections of the annihilation reactions $\bar{p}p \to \pi^+\pi^-\pi^0$, $\bar{p}p \to K^+K^-\pi^0$ and $\bar{p}p \to K^\pm K_S^0\pi^\mp$ in liquid (LH), normal pressure and temperature (NP) gas and low pressure (LP) gas hydrogen targets. The errors on the binned theoretical functions are summed to the experimental ones

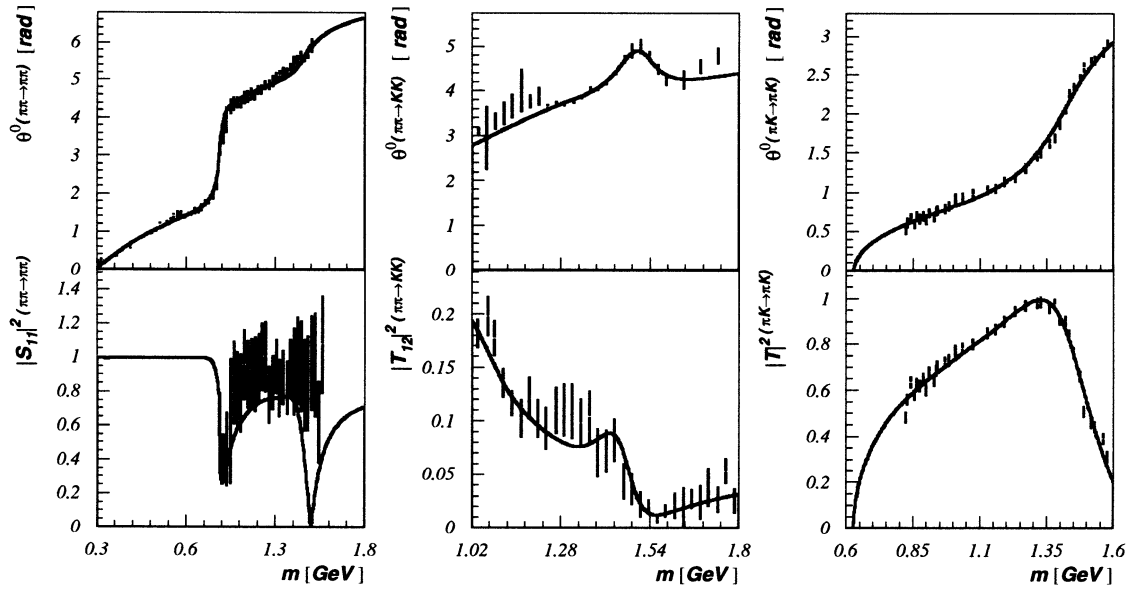

Fig. 5. Fit results on scattering data: phase shift (first row) and scattering amplitude squared (second row) of $\pi\pi \to \pi\pi$ (first column), $\pi\pi \to K\bar{K}$ (second column) and $\pi K \to \pi K$ (third column) S-wave scattering

multiplicative constant BR_j^k, the comparison, obtained by fitting this constants, shows a good agreement.

The products $W^k(\rho_t)\, BR_j^k$ obtained in this analysis represent new experimental information useful to determine the density dependence of the P-wave contribution. Following the procedure explained in [4] we fit the data set formed by the percentages of Table 2 and the sets "A" and "B-low" [4] consisting of $\pi^+\pi^-$, $\pi^0\pi^0$, $\pi^0\eta$, $\eta\eta$, K^+K^-, K_SK_L, K_SK_S, $\phi\pi^0$, $\eta(1440)\pi^+\pi^-$ branching ratios at different densities. Concerning the hyperfine levels we have considered two alternative hypotheses:

- statistical mixture (enhancement factors set to 1). We get a $\chi^2/n.d.f. = 3.07$ and the following P-wave percentages: 12.6 ± 0.8 (LH), 57.2 ± 1.5 (NP), 82.1 ± 2.0 (LP);
- deviation from statistical mixture (enhancement factors from [3]). We get a $\chi^2/n.d.f. = 3.00$ and the following P-wave percentages: 12.0 ± 0.9 (LH), 57.3 ± 1.5 (NP), 81.8 ± 2.0 (LP).

In both cases we obtain a good description of all experimental data except for the liquid P-wave three mesons branching ratios, as it is clear also from Fig. 6. These results are compatible within the experimental errors with the detailed analysis of [4]

6.2 Resonance partial widths and branching ratios

One of the fundamental advantages of a coupled channel analysis is the direct determination of the resonance partial widths and their ratios. In single channel analyses, on the contrary, the latter can be obtained only by calculating the resonance-spectator branching ratios in each final state. From (3), (4) and (14) we deduce that the branching ratio $BR_{j\alpha}^k(\rho_t)$ of the resonance-spectator α, from the partial wave k, in the final state j, at the density ρ_t is given by the following equation:

$$\begin{aligned} BR_{j\alpha}^k(\rho_t) &= W^k(\rho_t)\, |\hat{\beta}^k|^2 \sum_{pq} |\mathcal{F}_{pq\,j\alpha}^k|^2 \\ &= BR_j(\rho_t)\, \mathcal{P}_j^k(\rho_t)\, \frac{\sum_{pq} |\mathcal{F}_{pq\,j\alpha}^k|^2}{\sum_{pq} |\mathcal{F}_{pqj}^k|^2} \end{aligned} \qquad (15)$$

where $BR_j(\rho_t)$ and $\mathcal{P}_j^k(\rho_t)$ are expressed by (14) and listed in Table 2 and $\mathcal{F}_{pq\,j\alpha}^k$ is the amplitude associated to the physical state α, which has been extracted from the K-matrix and P-vector expression (7) of the production amplitude by means of the detailed procedure discussed in [12]. The ratio in the last equality represents the fraction $F_{j\alpha}^k$ of the resonance-spectator α, in the final state j from the partial wave k; its values are listed in Table 3. For instance, the $BR(\bar{p}p \to \rho(770)\pi, \rho \to \pi\pi)$ from ${}^1S_0$ in LH can be calculated as: $53.6 \times 10^{-3} \times 0.176 \times 0.197 = 1.86 \times 10^{-3}$. ((15) shows clearly that the resonance branching ratio should be calculated by normalizing the integral over the Dalitz-plot of the resonance α to the integral of the partial wave, which includes also the interference effects). From the previous discussion, it is clear that the direct determination of the resonance partial widths is more precise and avoids systematic uncertainties which can arise in the measurement of the final state branching ratios and in the partial wave deconvolution. In the following, both the discussed partial widths ratio determinations will be given. The eventual agreement has to be considered a consistency check of the whole analysis.

- f_0 *isobar.*
  As is known many of the properties of $f_0(980)$ are related to the closeness of its mass to the $K\bar{K}$ threshold. By studying the behaviour of the real and imaginary part of the inverse propagator matrix we determine a

Table 3. Resonance-spectator fractions $F^k_{j\alpha}$ (in units of 10^{-2}) from each final state and partial wave (physical background fractions are not listed)

Intermediate state	$\pi^+\pi^-\pi^0$	$K^+K^-\pi^0$	$K^\pm K^0_S\pi^\mp$	P.W.
$f_0(980)\pi^0$	19.2 ± 1.5	12.3 ± 2		$^1S_0$
	8.7 ± 2.4	17.7 ± 6		$^3P_1$
$f_0(1370)\pi^0$	20.4 ± 1.7	148 ± 9		$^1S_0$
	0.41 ± 0.21	0.36 ± 0.16		$^3P_1$
$f_0(1500)\pi^0$	19.8 ± 1.9	35.1 ± 1.8		$^1S_0$
	7.6 ± 2.2	21.3 ± 6.6		$^3P_1$
$K_0^*(1430)K$		53 ± 18	66 ± 12	$^1S_0$
		1.5 ± 1.0	6 ± 5	$^1P_1$
		24 ± 5	33 ± 4	$^3P_1$
$a_0(980)\pi$		9.2 ± 0.7	14.1 ± 1.0	$^1S_0$
$a_0(1300)\pi$		6.0 ± 0.6	9.9 ± 1.0	$^1S_0$
		$C-forbidden$	17.6 ± 2.1	$^1P_1$
		3.0 ± 0.3	4.1 ± 0.5	$^3P_1$
$\phi(1020)\pi^0$		28 ± 8		$^3S_1$
$K_1^*(892)K$		24 ± 5	35 ± 5	$^1S_0$
		58 ± 5	57 ± 7	$^3S_1$
		38 ± 6	29 ± 6	$^1P_1$
		57 ± 7	54 ± 5	$^3P_1$
		69 ± 12	79 ± 8	$^3P_2$
$\rho(770)\pi$	19.7 ± 2.8	$C-forbidden$	$<10^{-2}$	$^1S_0$
	133 ± 1.7	$<10^{-2}$	$<10^{-2}$	$^3S_1$
	10.5 ± 2.9	$<10^{-2}$	$<10^{-2}$	$^1P_1^{L=0}$
	85.0 ± 2.6	$<10^{-2}$	$<10^{-2}$	$^1P_1^{L=2}$
	33 ± 9	$C-forbidden$	$<10^{-2}$	$^3P_1^{L=0}$
	1.7 ± 0.7	$C-forbidden$	$<10^{-2}$	$^3P_1^{L=2}$
	22.6 ± 5.0	$C-forbidden$	$<10^{-2}$	$^3P_2$
$\rho(1450)\pi$	12.9 ± 2.2	$C-forbidden$	0.42 ± 0.08	$^1S_0$
	8.1 ± 2.5	0.25 ± 0.09	0.41 ± 0.11	$^3S_1$
	19.7 ± 9.0	0.73 ± 0.30	0.50 ± 0.22	$^1P_1^{L=0}$
	9.0 ± 6.0	0.27 ± 0.18	0.18 ± 0.09	$^1P_1^{L=2}$
	9.3 ± 6.0	$C-forbidden$	0.43 ± 0.25	$^3P_1^{L=0}$
	$<10^{-2}$	$C-forbidden$	$<10^{-2}$	$^3P_1^{L=2}$
	128 ± 3	$C-forbidden$	4.35 ± 0.30	$^3P_2$
$\rho(1700)\pi$	0.89 ± 0.10	$C-forbidden$	7.8 ± 0.6	$^1S_0$
	2.8 ± 0.2	25.5 ± 0.4	42.0 ± 0.8	$^3S_1$
	2.9 ± 0.2	50.8 ± 0.7	33.9 ± 0.3	$^1P_1^{L=0}$
	0.56 ± 0.08	4.2 ± 0.4	2.8 ± 0.4	$^1P_1^{L=2}$
	1.1 ± 0.2	$C-forbidden$	10.7 ± 1.7	$^3P_1^{L=0}$
	$<10^{-2}$	$C-forbidden$	$<10^{-2}$	$^3P_1^{L=2}$
	0.57 ± 0.12	$C-forbidden$	3.7 ± 0.8	$^3P_2$
$f_2(1270)\pi^0$	15.8 ± 0.7	5.0 ± 1.4		$^1S_0$
	35.5 ± 3.2	14.8 ± 3.2		$^3P_1$
	18.2 ± 1.1	10.7 ± 3.1		$^3P_2$
$f_2'(1525)\pi^0$	$<10^{-2}$	3.4 ± 0.7		$^1S_0$
	$<10^{-2}$	9.1 ± 0.7		$^3P_1$
	$<10^{-2}$	$12. \pm 3.0$		$^3P_2$
$f_2(1565)\pi^0$	13.1 ± 0.9	1.0 ± 0.3		$^1S_0$
	3.5 ± 0.9	0.4 ± 0.2		$^3P_1$
	53.2 ± 1.0	7.6 ± 2.0		$^3P_2$
$a_2(1320)\pi$		14 ± 3	22 ± 4	$^1S_0$
		$C-forbidden$	5 ± 2	$^3S_1$
		$C-forbidden$	7 ± 3	$^1P_1$
		5 ± 4	7 ± 5	$^3P_1$
		14 ± 8	13 ± 8	$^3P_2$

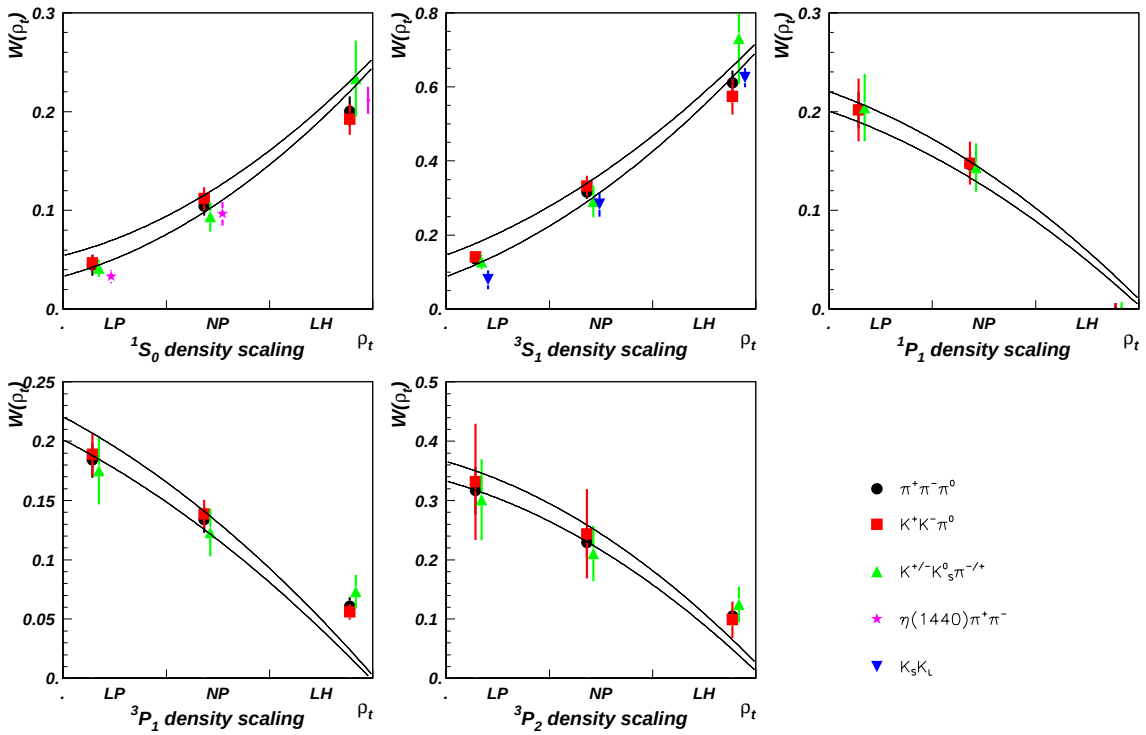

Fig. 6. Hydrogen density dependence of the annihilation frequency from each involved partial wave of the $\bar{p}p$ system. The continuous lines represent the region allowed by the different models considered in [3]. The experimental points corresponding to the same density were shifted to be better distinguishable

total width of $\Gamma = 174 \pm 10\,(MeV)$ reduced by the threshold effect to the value listed in Table 1 [12].
The physical state associated to $f_0(400{-}1200)$ looks like a very broad structure which departs completely from the Breit-Wigner shape and for this reason its fractions are not quoted. Also in this case, the physical pole parameters listed in Table 1 are obtained by calculating the imaginary part of the inverse propagator matrix at the mass value which zeroes its real part [12].
The $f_0(1370)$ turns out to be coupled mainly to the unobserved $\eta\eta$ and 4π channels. The following ratio of partial widths and branching ratios are obtained

$$\frac{\Gamma_{K\bar{K}}}{\Gamma_{\pi\pi}} = 0.91 \pm 0.20$$

$$\frac{BR(p\bar{p} \to f_0\,\pi^0,\, f_0 \to K\bar{K})}{BR(p\bar{p} \to f_0\,\pi^0,\, f_0 \to \pi\pi)} = \begin{cases} 1.00 \pm 0.20\ ^1S_0 \\ 0.94 \pm 0.20\ ^3P_1 \end{cases}$$

Concerning $f_0(1500)$ we get the following ratios of partial widths and branching ratios

$$\frac{\Gamma_{K\bar{K}}}{\Gamma_{\pi\pi}} = 0.25 \pm 0.03$$

$$\frac{BR(p\bar{p} \to f_0\pi^0, f_0 \to K\bar{K})}{BR(p\bar{p} \to f_0\pi^0, f_0 \to \pi\pi)} = \begin{cases} 0.24 \pm 0.04\ ^1S_0 \\ 0.30 \pm 0.04\ ^3P_1 \end{cases}$$

These values represent the first determination of $\Gamma_{K\bar{K}}/\Gamma_{\pi\pi}$ ratio obtained in the frame of a coupled channel analysis of annihilation data and agree with the recent determinations of [26] and [27]. Concerning the interpretation of $f_0(1500)$ the obtained partial width ratio and the ratio $\Gamma_{\eta\eta}/\Gamma_{\pi\pi}$ measured in [26] ($\Gamma_{\eta\eta}/\Gamma_{\pi\pi} = 0.157 \pm 0.060$) and [28] ($\Gamma_{\eta\eta}/\Gamma_{\pi\pi} = 0.182 \pm 0.027$) rule out both the pure gluonium an the $s\bar{s}$ hyphotesis and are compatible with the flavour composition of a conventional meson dominated by light quarks [29]. At present this interpretation is inconsistent with its non observation in $\gamma\gamma$ decay mode [36] ($\Gamma_{\gamma\gamma} < 1.08$ keV).

– a_0 *isobar.*
As the direct insight into the experimental data shows, $a_0(980)$ is produced mainly from S-wave. The analysis confirms the neglibile contribution of P-wave. By using the $a_0(980)$ production branching ratio measured in this analysis and in the previous Obelix analysis of the reaction $\bar{p}p \to \pi^+\pi^-\eta$ ($(8.2 \pm 0.5) \times 10^{-4}$ in LH) [30] we get the following ratio of partial widths: $\Gamma_{K\bar{K}}/\Gamma_{\eta\pi} = 0.23 \pm 0.04$ in agreement with the PDG [35].
The second pole observed in the $K\bar{K}$ decay mode has a mass around 1300 MeV and width (see Table 1) in agreement with the results of the previous OBELIX analysis ($M = 1290 \pm 10$ MeV [8]). Higher values of the mass [38] are ruled out by χ^2 (if a resonance mass value of 1450 MeV is fixed its fraction becomes negligible).

– $\phi(1020)$.
We confirm a strong $\phi(1020)$ production from $^3S_1$ partial wave and a negligible contribution of $^1P_1$. The measured branching ratio are $BR(p\bar{p} \to \phi\pi^0) = (5.0 \pm 1.8) \times 10^{-4}$ in LH, $(2.9 \pm 1.0) \times 10^{-4}$ at NP and $(1.2 \pm$

$0.4) \times 10^{-4}$ at LP, in agreement with the previous determination [32].

– $K^*(892)$.
The mass splitting of isospin dublet determined by the fit has the following value

$$M_{K^*(892)^0} - M_{K^*(892)^\pm} \;=\; (4 \pm 2)\, MeV \qquad (16)$$

The production of $K^*(892)$ is regulated by a dynamical selection rule which suppresses, in each partial wave, one of the two $\bar{p}p$ isospin sources. This result, clearly observed in S-wave by [24], is now measured, for the first time, also in P-wave. For instance, in the case of $K^+K^-\pi^0$ final state, where the K^* interference pattern is isospin independent, we get

$$\frac{BR(p\bar{p} \to K^*\,K, I=1)}{BR(p\bar{p} \to K^*\,K, I=0)} \;=\; \begin{cases} 0.40 \pm 0.07 & {}^1S_0 \\ 5.8 \pm 0.9 & {}^3S_1 \\ 0.25 \pm 0.02 & {}^1P_1 \\ 0.10 \pm 0.01 & {}^3P_1 \\ 5.03 \pm 0.34 & {}^3P_2 \end{cases}$$

Besides the necessity to understand the origin of this dynamical selection rule, interesting phenomena can be addressed to these results. For instance, the huge OZI-rule violating $\phi\pi$ production from ${}^3S_1$ and its suppression from ${}^1P_1$, can be related, through the $K^*(892)K$ rescattering in the final state, to the enhancement of K^*K production from $I=1$ and $I=0$ $\bar{p}p$ sources in ${}^3S_1$ and ${}^1P_1$ partial wave respectively [25].

– ρ *isobar.*
The mass splitting of the $\rho(770)$ isospin multiplet determined by the fit has the following value

$$M_{\rho(770)^0} - M_{\rho(770)^\pm} \;=\; (-2 \pm 4)\, MeV \qquad (17)$$

By means of Tables 2 and 4, averaging over the three densities, we get the following ratio of branching ratios

$$\frac{BR(p\bar{p} \to \rho^{\pm,0}\,\pi^{\mp,0},\, {}^3S_1)}{BR(p\bar{p} \to \rho^{\pm}\,\pi^{\mp},\, {}^1S_0)} \;=\; 25 \pm 5 \qquad (18)$$

which is the well known dynamical selection rule from S-waves i.e. $\rho\pi$ puzzle [23] (from P-waves such an evident effect is not observed). As pointed out in our previous paper [7] the enhancement of ρ production with relative angular momentum $L=2$ with respect to $L=0$ was observed in ${}^1P_1$ partial wave

$$\frac{BR(p\bar{p} \to \rho^{\pm,0}\,\pi^{\mp,0},\, {}^1P_1^{L=2})}{BR(p\bar{p} \to \rho^{\pm,0}\,\pi^{\mp,0},\, {}^1P_1^{L=0})} \;=\; 8.1 \pm 2.0 \qquad (19)$$

As previously said, $\rho(1450)$ is necessary to reproduce the shape of $\rho(770)$ bands, even though we got mass values remarkably lower than the PDG ones [35]. In a first set of fits we considered only $\pi\pi$ decay mode, getting the resonance parameters $M = 1227 \pm 30$ MeV and $\Gamma = 680 \pm 30$ MeV. The inclusion of 4π decay mode lowered the parameters to $M = 1182 \pm 30$ MeV and $\Gamma = 389 \pm 20$ MeV leaving nearly unchanged the other parameters since its contribution is limited to $\pi^+\pi^-\pi^0$ final state. In our opinion the measurement of the $\rho(1450)$ parameters in annihilation experiments still remains problematic, since the obtained mass values are systematically lower than the PDG mean value (With the exception of $\bar{p}$D annihililation mesurament of [33]).
The $\rho(1700)$ mass and width are compatible width our previous determination [8].

– f_2 *isobar.*
Concerning partial widths and branching ratios of $f_2(1270)$ we get the following ratios

$$\frac{\Gamma_{K\bar{K}}}{\Gamma_{\pi\pi}} = 0.045 \pm 0.010$$

$$\frac{BR(p\bar{p} \to f_2\,\pi^0,\, f_2 \to K\bar{K})}{BR(p\bar{p} \to f_2\,\pi^0,\, f_2 \to \pi\pi)} = \begin{cases} 0.043 \pm 0.010 & {}^1S_0 \\ 0.045 \pm 0.010 & {}^3P_1 \\ 0.048 \pm 0.010 & {}^3P_2 \end{cases}$$

which agree, within the experimental errors, with the PDG value [35].
As is known the ratio of the production branching ratios of $f_2'(1525)$ and $f_2(1270)$ can be used to determine possible OZI-rule violation effects in $J^{PC} = 2^{++}$, $I^G = 0^+$ [32,34], since $f_2'(1525)$ is nearly an $\bar{s}s$ state. By correcting for the unseen decay modes we get the following values

$$\frac{BR(p\bar{p} \to f_2'(1525)\pi^0)}{BR(p\bar{p} \to f_2(1270)\pi^0)} \;=\; \begin{cases} 0.028 \pm 0.006 & {}^1S_0 \\ 0.026 \pm 0.003 & {}^3P_1 \\ 0.051 \pm 0.020 & {}^3P_2 \end{cases}$$

to be compared to the OZI-rule theoretical expectation $R_{th} = \rho_{f_2'}/\rho_{f_2} \times\ tan^2(\theta_{2^{++}} - \theta_{id}) = 0.022$ ($\theta_{2^{++}} = 28^o$ [35]). Our values seem not to require strong OZI-rule violation effects from S and P waves. As far as P-waves is concerned, the disagreement with [32] can be addressed to the $f_2(1700)$ resonance, which is not required by the present analysis.
The third pole corresponding to $f_2(1565)$, mainly required by pion data, turns out to have a negligible $K\bar{K}$ coupling. Moreover due to the fact that no indications are available on the important 4π decay mode we set to zero its 4π k-matrix decay width. For these reasons only the mass and the total width of the resonance can be measured by the present analysis (see Table 1). Although this resonance is very close to $f_2'(1525)$, its larger width and different coupling make the two signals distinguishable. Its dominant production from ${}^3P_2$ partial wave is observed and confirms our previous determination [7].

– $a_2(1320)$.
In the present analysis the $a_2(1320)$ is observed both in K^+K^- and in $K^\pm K^0$ channels. This fact allows us to remark a conceptual aspect in branching ratio calculations. In fact Clebsch-Gordan coefficients determine the ratio $R = BR(\bar{p}p \to a_2^+(1320)\pi^-,\, a_2^+(1320) \to K^+\bar{K}^0)/\ BR(\bar{p}p \to a_2^0(1320)\pi^0,\, a_2^0(1320) \to K^+K^-)$

$= 2$ in each partial wave, which can be checked also by the analysis. If the integral over the Dalitz-plot of $a_2(1320)$ is correctly normalized to the partial wave integral we obtain $R(^1S_0) = 1.59 \pm 0.35$, $R(^3P_1) = 1.61 \pm 0.35$ and $R(^3P_2) = 1.62 \pm 0.35$, which are compatible with the expected value. The calculation performed by neglecting the interference effects would give respectively $R(^1S_0) = 19 \pm 3$, $R(^3P_1) = 10 \pm 5$ and $R(^3P_2) = 2.7 \pm 0.6$.

From Tables 2,4 we get the following values of $BR(p\bar{p} \to a_2(1320)^+\pi^-\,;\, a_2^+ \to K^+\bar{K}^0)$: LH, $(3.88 \pm 0.90) \times 10^{-4}$; $^1S_0$ of LH, $(2.45 \pm 0.50) \times 10^{-4}$. Both the values agree within the errors with the bubble chamber [24] and Crystal Barrel [38,39] measurements. From the analysis of $p\bar{p} \to \pi^+\pi^-\eta$ [30] we can calculate the $BR(p\bar{p} \to a_2(1320)^+\pi^-\,;\, a_2^+ \to \eta\pi^+)$: LH, $(37.2 \pm 3.4) \times 10^{-4}$; $^1S_0$ of LH, $(23.7 \pm 1.9) \times 10^{-4}$, which agree with [41]. In spite of the consistency among these experimental measurements, the $a_2(1320)$ decay ratio is $\Gamma_{K\bar{K}}/\Gamma_{\eta\pi} = 0.10 \pm 0.02$, which is about a factor 3 lower than the PDG one. From the analysis of $p\bar{p} \to \pi^+\pi^-\pi^+\pi^-$ [40] we can also calculate $BR(p\bar{p} \to a_2(1320)^+\pi^-\,;\, a_2^+ \to \rho^0\pi^+)$: LH, $(51.0 \pm 5.0) \times 10^{-4}$; $^1S_0$ of LH, $(37.1 \pm 4.0) \times 10^{-4}$. Correcting for the unobserved $\rho^+\pi^0$ decays we can determine the ratio $\Gamma_{K\bar{K}}/\Gamma_{\rho\pi} = 0.036 \pm 0.07$ by using LH or 0.032 ± 0.007 by using $^1S_0$ in LH, which is a factor of 2 lower than PDG. From this scenario it is not clear which decay channel is responsible for the discrepancy with PDG.

7 Conclusions

A coupled channel analysis of $\pi^+\pi^-\pi^0$, $K^+K^-\pi^0$ and $K^\pm K^0_S\pi^\mp$ final states produced by $\bar{p}p$ annihilation at rest in hydrogen targets has been performed. The relevant features of the present analysis are the following:

- each hadronic final state is observed in different partial wave mixtures dominated by S-wave (LH), P-wave (LP) or comparable S and P-wave fractions (NP) of the $\bar{p}p$ system. In this way a precise control over the shape and contribution of each involved partial wave is obtained. The comparison of their percentages with other independent determinations (two meson branching ratios) shows a satisfactory agreement;
- a decisive improvement in the disentanglement of I=0 and I=1 resonances in $K^+K^-\pi^0$ final state is obtained by introducing the $K^\pm K^0_S\pi^\mp$ channel. In this way a better control on the $K\bar{K}$ resonance decay mode is obtained;
- in order to improve the description of $J^P = 0^+$ isobars $I = 0$, $\pi\pi$, $K\bar{K}$ and I=1/2 $K\pi$ scattering data are included;
- all the experimental data are analyzed by means of a unitary formalism in the framework of the K-matrix and P-vector approach.

The results concern mainly masses, total widths, partial widths and fractions of all the involved resonances:

- dynamical selection rules have been confirmed in $\rho(770)\pi$ production from S-wave ($\rho\pi$ puzzle) and from $^1P_1$ partial wave (enhanced production from L=2 component with respect to L=0). Dynamical selection rules are responsible also for the dominant S-wave production of $\phi(1020)\pi^0$ and $a_0(980)\pi$. The dominant production of $K^*(892)K$ from one isospin source of the $\bar{p}p$ system is clearly observed in S-wave and, for the first time, also in P-wave;
- possible OZI-rule violation effects have been explored in the $J^{PC} = 2^{++}$ nonet. The obtained ratios of $f_2'(1525)\pi^0$ and $f_2(1270)\pi^0$ production exclude strong OZI-rule violation effects.
- the relevant $\Gamma_{K\bar{K}}/\Gamma_{\pi\pi}$ ratios have been calculated by means of two independent procedures which agree within the errors. In the case of $f_0(1500)$ we get the improved measurement $\Gamma_{K\bar{K}}/\Gamma_{\pi\pi} = 0.25 \pm 0.03$ [35]. A dominant $s\bar{s}$ component of the meson can be excluded by combining this result with the measurement of $\Gamma_{\eta\eta}/\Gamma_{\pi\pi}$, however the $\Gamma_{\gamma\gamma}$ suppression cannot be explained. A deeper comprehension of this resonance can be obtained by invoking a mixing scheme between gluonium and quarkonium components [29,37]. The $f_0(1370)$ ($M = 1373 \pm 10$ MeV; $\Gamma = 274 \pm 20$ MeV) is clearly required in the present analysis and the ratio $\Gamma_{K\bar{K}}/\Gamma_{\pi\pi} = 0.91 \pm 0.20$ is measured;
- by this extended analysis, we confirm the previous $a_0(1300)$ OBELIX determination [8] ($M = 1303 \pm 16$ MeV; $\Gamma = 92 \pm 16$ MeV). Also the present determinations of $\rho(1450)$ ($M = 1182 \pm 30$ MeV; $\Gamma = 389 \pm 20$ MeV) and $\rho(1700)$ ($M = 1594 \pm 20$ MeV; $\Gamma = 259 \pm 20$ MeV) agree with our previous analyses [7,8].

Acknowledgements. We would like to thank for the useful discussions C. Amsler and E. Klempt.

Appendix

This section is devoted to the description of the structure of the production amplitudes. The resonances of the same isobar are indicated by their general PDG names (for instance f_0 indicates the set of resonances $f_0(980)$, $f_0(1370)$, $f_0(1500)$ and $f_0(400-1200)$) taking in mind that its meaning depends on the considered final state (f_0 means $\pi^+\pi^-$ in $\pi^+\pi^-\pi^0$ and K^+K^- in $K^+K^-\pi^0$ final states respectively). Isospinor and isovector multiplets have the well known expressions while isospinor antimultiplets are defined as $\bar{K} = (-\bar{K}^0, K^-)$ in order to have the same composition coefficients of the multiplets.

The general $\pi\pi\pi$ and $K\bar{K}\pi$ production amplitudes have been written projecting each $\bar{p}p$ initial state on all the possible resonance-spectator states (the resonances considered in this analysis are listed in Table 4). The amplitudes with the correct symmetry properties are obtained by means of G-parity transformations and permutations of identical particles.

The detailed structure of the amplitude in each final state and partial wave is given in Tables 5–9. The $\bar{p}p$

Table 4. Isobars (I^G, J^{PC}) considered in the present analysis

	Resonance							
Decay Mode	$(0^+, 0^{++})$	$(1/2, 0^+)$	$(1^-, 0^+)$	$(0^-, 1^{--})$	$(1/2, 1^-)$	$(1^+, 1^-)$	$(0^+, 2^{++})$	$(1^-, 2^+)$
	f_0	K_0^*	a_0	ϕ	K_1^*	ρ	f_2	a_2
$\pi\pi$	×					×	×	
$K\bar{K}$	×		×	×		×	×	×
$\pi K\, \pi\bar{K}$		×			×			

Table 5. Amplitudes for $\bar{p}p\ ^1S_0$ partial wave

$I^G J^{PC}$	*Res.*	L^c	$\pi^+\pi^-\pi^0$	$K^+K^-\pi^0$	$K^+\bar{K}^0\pi^-$
0^+0^{-+}	K_0^*	0	–	$-\frac{K_0^{*+}K_0^- + K_0^{*-}K_0^+}{\sqrt{12}}$	$-\frac{K_0^{*0}\bar{K}_0^0 + K_0^{*-}K_0^+}{\sqrt{6}}$
0^+0^{-+}	K_1^*	1	–	$-\frac{K_1^{*+}K_1^- + K_1^{*-}K_1^+}{\sqrt{12}}$	$-\frac{K_1^{*0}\bar{K}_1^0 + \bar{K}_1^{*-}K_1^+}{\sqrt{6}}$
0^+0^{-+}	a_0	0	–	$-\frac{1}{\sqrt{6}}a_0^0\pi^0$	$-\frac{1}{\sqrt{3}}a_0^+\pi^-$
0^+0^{-+}	a_2	2	–	$-\frac{1}{\sqrt{6}}a_2^0\pi^0$	$-\frac{1}{\sqrt{3}}a_2^+\pi^-$
1^-0^{-+}	f_0	0	$\sqrt{\frac{2}{3}}f_0\pi^0$	$\frac{1}{\sqrt{2}}f_0\pi^0$	–
1^-0^{-+}	f_2	2	$\sqrt{\frac{2}{3}}f_2\pi^0$	$\frac{1}{\sqrt{2}}f_2\pi^0$	–
1^-0^{-+}	K_0^*	0	–	$-\frac{K_0^{*+}K_0^- + K_0^{*-}K_0^+}{\sqrt{12}}$	$\frac{K_0^{*0}\bar{K}_0^0 - K_0^{*-}K_0^+}{\sqrt{6}}$
1^-0^{-+}	K_1^*	1	–	$-\frac{K_1^{*+}K_1^- + K_1^{*-}K_1^+}{\sqrt{12}}$	$\frac{K_1^{*0}\bar{K}_1^0 - K_1^{*-}K_1^+}{\sqrt{6}}$
1^-0^{-+}	ρ	1	$\frac{\rho^-\pi^+ - \rho^+\pi^-}{\sqrt{2}}$	–	$-\frac{1}{\sqrt{2}}\rho^+\pi^-$

Table 6. Amplitudes for $\bar{p}p\ ^3S_1$ partial wave

$I^G J^{PC}$	*Res.*	L^c	$\pi^+\pi^-\pi^0$	$K^+K^-\pi^0$	$K^+\bar{K}^0\pi^-$
0^-1^{--}	K_1^*	1	–	$-\frac{K_1^{*+}K_1^- - K_1^{*-}K_1^+}{\sqrt{12}}$	$-\frac{K_1^{*0}\bar{K}_1^0 - \bar{K}_1^{*-}K_1^+}{\sqrt{6}}$
0^-1^{--}	ρ	1	$\frac{\rho^-\pi^+ + \rho^+\pi^- - \rho^0\pi^0}{\sqrt{3}}$	$-\frac{1}{\sqrt{6}}\rho^0\pi^0$	$-\frac{1}{\sqrt{3}}\rho^+\pi^-$
1^+1^{--}	K_1^*	1	–	$-\frac{K_1^{*+}K_1^- - K_1^{*-}K_1^+}{\sqrt{12}}$	$\frac{K_1^{*0}\bar{K}_1^0 + \bar{K}_1^{*-}K_1^+}{\sqrt{6}}$
1^+1^{--}	a_2	2	–	–	$-\frac{1}{\sqrt{2}}a_2^+\pi^-$
1^+1^{--}	ϕ	1	–	$\frac{1}{\sqrt{2}}\phi\pi^0$	–

Table 7. Amplitudes for $\bar{p}p\ ^1P_1$ partial wave

$I^G J^{PC}$	*Res.*	L^c	$\pi^+\pi^-\pi^0$	$K^+K^-\pi^0$	$K^+\bar{K}^0\pi^-$
0^-1^{+-}	K_0^*	1	–	$-\frac{K_0^{*+}K_0^- - K_0^{*-}K_0^+}{\sqrt{12}}$	$-\frac{K_0^{*0}\bar{K}_0^0 - \bar{K}_0^{*-}K_0^+}{\sqrt{6}}$
0^-1^{+-}	K_1^*	0, 2	–	$-\frac{K_1^{*+}K_1^- - K_1^{*-}K_1^+}{\sqrt{12}}$	$-\frac{K_1^{*0}\bar{K}_1^0 - \bar{K}_1^{*-}K_1^+}{\sqrt{6}}$
0^-1^{+-}	ρ	0, 2	$\frac{\rho^-\pi^+ + \rho^+\pi^- - \rho^0\pi^0}{\sqrt{3}}$	$-\frac{1}{\sqrt{6}}\rho^0\pi^0$	$-\frac{1}{\sqrt{3}}\rho^+\pi^-$
1^+1^{+-}	K_0^*	1	–	$-\frac{K_0^{*+}K_0^- - K_0^{*-}K_0^+}{\sqrt{12}}$	$\frac{K_0^{*0}\bar{K}_0^0 + \bar{K}_0^{*-}K_0^+}{\sqrt{6}}$
1^+1^{+-}	K_1^*	0, 2	–	$-\frac{K_1^{*+}K_1^- - K_1^{*-}K_1^+}{\sqrt{12}}$	$\frac{K_1^{*0}\bar{K}_1^0 + \bar{K}_1^{*-}K_1^+}{\sqrt{6}}$
1^+1^{+-}	a_0	1	–	–	$-\frac{1}{\sqrt{2}}a_0^+\pi^-$
1^+1^{+-}	a_2	1	–	–	$-\frac{1}{\sqrt{2}}a_2^+\pi^-$
1^+1^{+-}	ϕ	0, 2	–	$\frac{1}{\sqrt{2}}\phi\pi^0$	–

Table 8. Amplitudes for $\bar{p}p\ ^3P_1$ partial wave

I^GJ^{PC}	*Res.*	L^c	$\pi^+\pi^-\pi^0$	$K^+K^-\pi^0$	$K^+\bar{K}^0\pi^-$
0^+1^{++}	K_0^*	1	–	$-\frac{K_0^{*+}K_0^- + K_0^{*-}K_0^+}{\sqrt{12}}$	$-\frac{K_0^{*0}\bar{K}_0^0 + K_0^{*-}K_0^+}{\sqrt{6}}$
0^+1^{++}	K_1^*	0, 2	–	$-\frac{K_1^{*+}K_1^- + K_1^{*-}K_1^+}{\sqrt{12}}$	$-\frac{K_1^{*0}\bar{K}_1^0 + \bar{K}_1^{*-}K_1^+}{\sqrt{6}}$
0^+1^{++}	a_0	1	–	$-\frac{1}{\sqrt{6}}a_0^0\pi^0$	$-\frac{1}{\sqrt{3}}a_0^+\pi^-$
0^+1^{++}	a_2	1	–	$-\frac{1}{\sqrt{6}}a_2^0\pi^0$	$-\frac{1}{\sqrt{3}}a_2^+\pi^-$
1^-1^{++}	f_0	1	$\sqrt{\frac{2}{3}}f_0\pi^0$	$\frac{1}{\sqrt{2}}f_0\pi^0$	–
1^-1^{++}	f_2	1	$\sqrt{\frac{2}{3}}f_2\pi^0$	$\frac{1}{\sqrt{2}}f_2\pi^0$	–
1^-1^{++}	K_0^*	1	–	$-\frac{K_0^{*+}K_0^- + K_0^{*-}K_0^+}{\sqrt{12}}$	$\frac{K_0^{*0}\bar{K}_0^0 - K_0^{*-}K_0^+}{\sqrt{6}}$
1^-1^{++}	K_1^*	0, 2	–	$-\frac{K_1^{*+}K_1^- + K_1^{*-}K_1^+}{\sqrt{12}}$	$\frac{K_1^{*0}\bar{K}_1^0 - \bar{K}_1^{*-}K_1^+}{\sqrt{6}}$
1^-1^{++}	ρ	0, 2	$\frac{\rho^-\pi^+ + \rho^+\pi^-}{\sqrt{2}}$	–	$-\frac{1}{\sqrt{2}}\rho^+\pi^-$

Table 9. Amplitudes for $\bar{p}p\ ^3P_2$ partial wave

I^GJ^{PC}	*Res.*	L^c	$\pi^+\pi^-\pi^0$	$K^+K^-\pi^0$	$K^+\bar{K}^0\pi^-$
0^+2^{++}	K_1^*	2	–	$-\frac{K_1^{*+}K_1^- + K_1^{*-}K_1^+}{\sqrt{12}}$	$-\frac{K_1^{*0}\bar{K}_1^0 + \bar{K}_1^{*-}K_1^+}{\sqrt{6}}$
0^+2^{++}	a_2	1	–	$-\frac{1}{\sqrt{6}}a_2^0\pi^0$	$-\frac{1}{\sqrt{3}}a_2^+\pi^-$
1^-2^{++}	f_2	1	$\sqrt{\frac{2}{3}}f_2\pi^0$	$\frac{1}{\sqrt{2}}f_2\pi^0$	–
1^-2^{++}	K_1^*	2	–	$-\frac{K_1^{*+}K_1^- + K_1^{*-}K_1^+}{\sqrt{12}}$	$\frac{K_1^{*0}\bar{K}_1^0 - \bar{K}_1^{*-}K_1^+}{\sqrt{6}}$
1^-2^{++}	ρ	2	$\frac{\rho^-\pi^+ - \rho^+\pi^-}{\sqrt{2}}$	–	$-\frac{1}{\sqrt{2}}\rho^+\pi^-$

quantum numbers are listed in the first column while the general PDG name of the resonance and the resonance-spectator relative angular momentum are listed in the second and third columns respectively. The isospin coefficients arising from the production and decay processes and the interference patterns in each final state are indicated in the last three columns.

References

1. C.J. Batty, Rep. Prog. Phys. **52**, 1165 (1989)
2. G. Reifenrother, E. Klempt, Nucl. Phys. A **503**, 885 (1989); E. Borie, M. Leon, Phys. Rev. A **21**, 1460 (1980)
3. C.J. Batty, Nucl. Phys. A **601**, 425 (1996)
4. G. Bendiscioli et al., Nucl. Phys. A **686**, 317 (2001)
5. G. Grayer et al., Nucl. Phys. B **75**, 189 (1974); A. Etkin et al., Phys. Rev. D **25**, 1786 (1982); D. Aston et al., Nucl. Phys. B **296**, 493 (1988)
6. A. Adamo et al., Soviet Journal of Nuclear Physics **55**, 1732 (1992)
7. A. Bertin et al., Phys. Lett. B **408**, 476 (1997)
8. A. Bertin et al., Phys. Lett. B **434**, 180 (1998)
9. N. Semprini-Cesari for the Obelix Collaboration, LEAP '94, Proceedings of the Biennial Conference on Low-Energy Antiproton Physics, Bled, Slovenia, edited by G. Kernel et al., p.130
10. J. Harte, R.G. Saxchs, Phys. Rev. **135**, B459 (1964)
11. R.M. Sternheimer, S.I. Lindenbaum, Phys. Rev. **123**, 333 (1961); S. Mandelstam et al., Ann. Phys. **18**, 198 (1962)
12. M. Bargiotti et al., EPJdirect A **2**, 1 (2002)
13. C. Zemach, Phys. Rev. **133**, 1201 (1964); C. Zemach, Phys. Rev. **140**, 97 (1965); C. Zemach, Phys. Rev. **140**, 109 (1965)
14. F.V. Hippel, C. Quigg, Phys. Rev. D **5**, 624 (1972)
15. V.V. Anisovich, Yu.D. Prokoshkin, A.V. Sarantsev, Phys. Lett. B **389**, 388 (1996)
16. S. Weinberg, Phys. Rev. Lett. **17**, 616 (1966)
17. K.L. Au, D. Morgan, M.R. Pennington, Phys. Rev. D **35**, 1633 (1987)
18. M.R. Pennington, Proceedings of HADRON '95 Conference, Manchester, UK, Ed. M.C. Birse et al., 3, 1995
19. A.M. Badalyan, L.P. KOK, M.I. Polikarpov, Y.A. Simonov, Phys. Lett. B **82**, 31 (1982)
20. I.J.R. Aitchinson, Nucl. Phys. A **189**, 417 (1972); S.U. Chung et al.Ann. Phys **4**, 404 (1995)
21. A. Bertin et al., Phys. Lett. B **386**, 486 (1996)
22. A. Bertin et al., Phys. Lett. B **385**, 493 (1996)
23. B. May et al., Z. Phys. C **46**, 191 (1990); B. May et al., Z. Phys. C **46**, 203 (1990)
24. B. Conforto et al., Nucl. Phys. B **3**, 469 (1967); A. Bettini et al., Nuovo Cimento **A63**, 1199 (1969)
25. O. Gortchakov, M.P. Locher, V.E. Markushin, S. von Rotz, Z. Phys. A **353**, 447 (1996)
26. C. Amsler et al., Phys. Lett. B **355**, 425 (1995); A. Abele et al., Phys. Lett. B **385**, 425 (1996)
27. D. Barberis et al., Phys. Lett. B **462**, 462 (1999)

28. D. Barberis et al., Phys. Lett. B **479**, 59 (2000)
29. C. Amsler, F. Close, Phys. Rev. D **53**, 295 (1995); C. Amsler et al., private communication
30. R. Spighi for the Obelix Colaboration,Nucl. Phys. A **655**, 35c (1999); M. Villa for the Obelix Collaboration, in WHS99, Proceedings of Workshop on Hadron Spectroscopy, Frascati, Italy, Ed. by T. Bressani et al., 37
31. A. Filippi et al., Phys. Lett. B **495**, 284 (2000)
32. A. Alberico et al., Phys. Lett. B **438**, 430 (1998)
33. A. Abele et al., Phys. Lett. B **391**, 191 (1997). A. Abele et al., Phys. Lett. B **450**, 275 (1999)
34. C. Amsler et al., The Eur. Phys. Jour. C **23**, 29 (2002)
35. Review of Particle Physics, The Eur. Phys. Jour. C **15**, 1 (2000)
36. M. Acciarri et al., Phys. Lett. B **501**, 173 (2001); R. Barate et al., Phys. Lett. B **472**, 189 (2000)
37. F. Close, G. Farrar, Z.P. Li, Phys. Rev. D **55**, 5749 (1997); D. Weingarten Nucl. Phys. Proc. Suppl. **53**, 232 (1997); M. Genovese Phys. Rev. D **46**, 5204 (1992); V.V. Anisovich, V.A. Nikonov, A.V. Sarantsev hep-ph/0108188 , (2001); F. Close, A. Kirk, Phys. Lett. B **483**, 345 (2000)
38. A. Abele et al., Phys. Rev. D **57**, 3860 (1998)
39. S. von Dombrowski, PhD Thesis, Zurich University (1995); A. Abele et al., Phys. Lett. B **385**, 425 (1996)
40. A. Bertin et al., Phys. Lett. B **414**, 220 (1997); G. Bendiscioli et al., in preparation
41. C. Amsler et al., Phys. Lett. B **333**, 277 (1994); C. Amsler et al., Phys. Lett. B **355**, 425 (1995)